Integrating $^{40}Ar/^{39}Ar$, U-Pb, and astronomical clocks in the Cretaceous Niobrara Formation, Western Interior Basin, USA

Bradley B. Sageman[1†], Brad S. Singer[2], Stephen R. Meyers[2], Sarah E. Siewert[2,3], Ireneusz Walaszczyk[4], Daniel J. Condon[5], Brian R. Jicha[2], John D. Obradovich[6§], and David A. Sawyer[6]

[1]*Department of Earth and Planetary Sciences, Northwestern University, 2145 Sheridan Rd., Evanston, Illinois 60208, USA*
[2]*Department of Geoscience, University of Wisconsin–Madison, 1215 West Dayton St., Madison, Wisconsin 53706, USA*
[3]*British Petroleum, Houston, Texas 77079-2696, USA*
[4]*Faculty of Geology, University of Warsaw, Al. Zwirki i Wigury 92, PL-02-089, Warszawa, Poland*
[5]*NERC Isotope Geosciences Laboratory, British Geological Survey, Keyworth NG12 5GG, UK*
[6]*U.S. Geological Survey, MS 980, Denver, Colorado 80225, USA*

ABSTRACT

This study revises and improves the chronostratigraphic framework for late Turonian through early Campanian time based on work in the Western Interior U.S. and introduces new methods to better quantify uncertainties associated with the development of such time scales. Building on the unique attributes of the Western Interior Basin, which contains abundant volcanic ash beds and rhythmic strata interpreted to record orbital cycles, we integrate new radioisotopic data of improved accuracy with a recently published astrochronologic framework for the Niobrara Formation. New $^{40}Ar/^{39}Ar$ laser fusion ages corresponding to eight different ammonite biozones are determined by analysis of legacy samples, as well as newly collected material. These results are complemented by new U-Pb (zircon) chemical abrasion–isotope dilution–thermal ionization mass spectrometry ages from four biozones in the study interval. When combined with published radioisotopic data from the Cenomanian-Turonian boundary, paired $^{206}Pb/^{238}U$ and $^{40}Ar/^{39}Ar$ ages spanning Cenomanian to Campanian time support an astronomically calibrated Fish Canyon sanidine standard age of 28.201 Ma. Stage boundary ages are estimated via integration of new radioisotopic data with the floating astrochronology for the Niobrara Formation. The ages are determined by anchoring the long eccentricity bandpass from spectral analysis of the Niobrara Formation to radioisotopic ages with the lowest uncertainty proximal to the boundary, and adding or subtracting time by parsing the 405 k.y. cycles. The new stage boundary age determinations are: 89.75 ± 0.38 Ma for the Turonian-Coniacian, 86.49 ± 0.44 Ma for the Coniacian-Santonian, and 84.19 ± 0.38 Ma for the Santonian-Campanian boundary. The 2σ uncertainties for these estimates include systematic contributions from the radioisotopic measurements, astrochronologic methods, and geologic uncertainties (related to stratigraphic correlation and the presence of hiatuses). The latter geologic uncertainties have not been directly addressed in prior time scale studies and their determination was made possible by critical biostratigraphic observations. Each methodological approach employed in this study—new radioisotopic analysis, stratigraphic correlation, astrochronology, and ammonite and inoceramid biostratigraphy—was critical for achieving the final result.

INTRODUCTION

Cretaceous strata have long been a target of intense interest because they preserve paleoenvironmental, paleobiological, and geochemical records of sustained global warming, high sea level, rapid faunal turnover, mass extinctions, and perturbations of the carbon cycle known as oceanic anoxic events (e.g., Skelton, 2003). Floating astronomical time scales (ATS) for portions of the Cretaceous have begun to provide the resolution necessary to resolve these rapid environmental fluctuations and biological changes (e.g., Meyers et al., 2001; Grippo et al., 2004; Sageman et al., 2006; Locklair and Sageman, 2008; Huang et al., 2010; Hinnov and Hilgen, 2012), but to establish a global high-resolution time scale, floating astrochronologic age models must be integrated with established biostratigraphic/chemostratigraphic frameworks and anchored with accurate and precise radioisotopic ages (e.g., Meyers et al., 2012). The integration of new radioisotopic age determinations with high-resolution astrochronologies offers the most powerful tool to refine geologic time and interpolate ages for significant deep-time geologic events, such as stage and biozone boundaries.

Since the pioneering work of Obradovich (1993), the Cretaceous part of the geologic time scale has been chiefly based on his $^{40}Ar/^{39}Ar$ dating of altered volcanic ash beds (bentonites) from the Western Interior Basin of the U.S. These bentonites are well documented within the Cretaceous ammonite biostratigraphy of Cobban (1993), and although several of the ages have been used in the past to help constrain an orbital signature in the rock record (e.g., Sageman et al., 1997; Meyers et al., 2001; Locklair and Sageman, 2008), the analytical uncertainty associated with the original $^{40}Ar/^{39}Ar$ ages does not meet the desired threshold for calibration of astrochronologic age models for the Cretaceous (Hinnov and Ogg, 2007; Meyers et al., 2012). Recent advances in the $^{40}Ar/^{39}Ar$ and U-Pb methods, including improved standardization and inter-laboratory calibration (e.g., Mattinson, 2005; Condon et al., 2007; Kuiper et al., 2008; Renne et al., 2010; Schmitz, 2012), now enable better than 3 per mil (‰) total uncertainty on radioisotopic ages throughout the Cretaceous, facilitating the integration of data derived from multiple independent chronometers (e.g., Smith et al., 2010; Meyers et al., 2012; ; Renne et al., 2013).

The purpose of the present study is threefold. First, we refine and improve the chronostratigraphic framework for late Turonian through

†E-mail: brad@earth.northwestern.edu.
§Deceased.

GSA Bulletin; July/August 2014; v. 126; no. 7/8; p. 956–973; doi:10.1130/B30929.1; 7 figures; 3 tables; Data Repository item 2014122; published online 20 March 2014.

early Campanian strata of the Western Interior Basin (represented mainly by the Niobrara Formation and its equivalents) by integrating new radioisotopic age data, predominantly from Montana, with an existing astrochronologic age model developed from Denver Basin cores (Locklair and Sageman, 2008). The integration is fundamentally facilitated by updated biostratigraphy (e.g., Cobban et al., 2006; Walaszczyk and Cobban, 2006). The geochronology, which employs $^{40}Ar/^{39}Ar$ and U-Pb techniques on sanidine and zircon collected from ash beds spanning the late Turonian *Prionocyclus macombi* through early Campanian *Scaphites hippocrepis* II biozones (Fig. 1), significantly improves accuracy and precision of $^{40}Ar/^{39}Ar$ ages and importantly adds U-Pb ages (for four of the Niobrara ashes) where none existed previously. The work includes re-analysis of Obradovich (1993) legacy samples as well as analysis of newly collected material from the same ash horizons, and is thus directly linked to the previous $^{40}Ar/^{39}Ar$ time scale for the study interval. In addition to eight ages representing six biozones within the Niobrara Formation (three of the dated ashes, corresponding to sites 5–7 in Fig. 1, occur within the *Scaphites depressus* biozone), we provide new $^{40}Ar/^{39}Ar$ ages for two Late Turonian biozones (sites 9–11, in Fig. 1, also indicated in Fig. 2) that underlie the Niobrara (*Scaphites nigricollensis* and *Prionocyclus macombi*), and help to constrain the total duration of Niobrara deposition.

Second, the acquisition of paired $^{40}Ar/^{39}Ar$ and U-Pb ages is significant because it allows an evaluation of various ^{40}K decay constants and associated ages proposed for the widely used Fish Canyon sanidine (FCs) neutron fluence monitor for the $^{40}Ar/^{39}Ar$ system, specifically the estimates of 28.02 Ma (Renne et al., 1998), 28.201 Ma (Kuiper et al., 2008), and 28.294 Ma (Renne et al., 2011). Four new paired $^{40}Ar/^{39}Ar$ and U-Pb ages from the present study are combined with three from the Cenomanian-Turonian boundary interval (presented in Meyers et al., 2012) to provide a data set to evaluate the proposed FCs ages. The application of a unified and consistent analytical approach—with careful consideration of potential sources of uncertainty (e.g., inheritance of older crystals, loss of radiogenic daughter products)—makes this data set pertinent to ongoing efforts to improve the accuracy of $^{40}Ar/^{39}Ar$ geochronology.

Ash beds from the study interval were mainly sampled in Montana because they occur there within fossiliferous sections that have detailed biostratigraphy, and they tend to be more abundant, thicker, and crystal rich in this part of the basin (e.g., Obradovich, 1993). Linking the new age data to an astrochronologic framework is important because the latter provides a means to more accurately quantify time between dated horizons. In order to integrate dated ash beds sampled in Montana with the Niobrara floating astrochronology developed in Colorado, we employ biostratigraphic and lithostratigraphic correlation techniques. The biozone data play a critical role in this process and have allowed

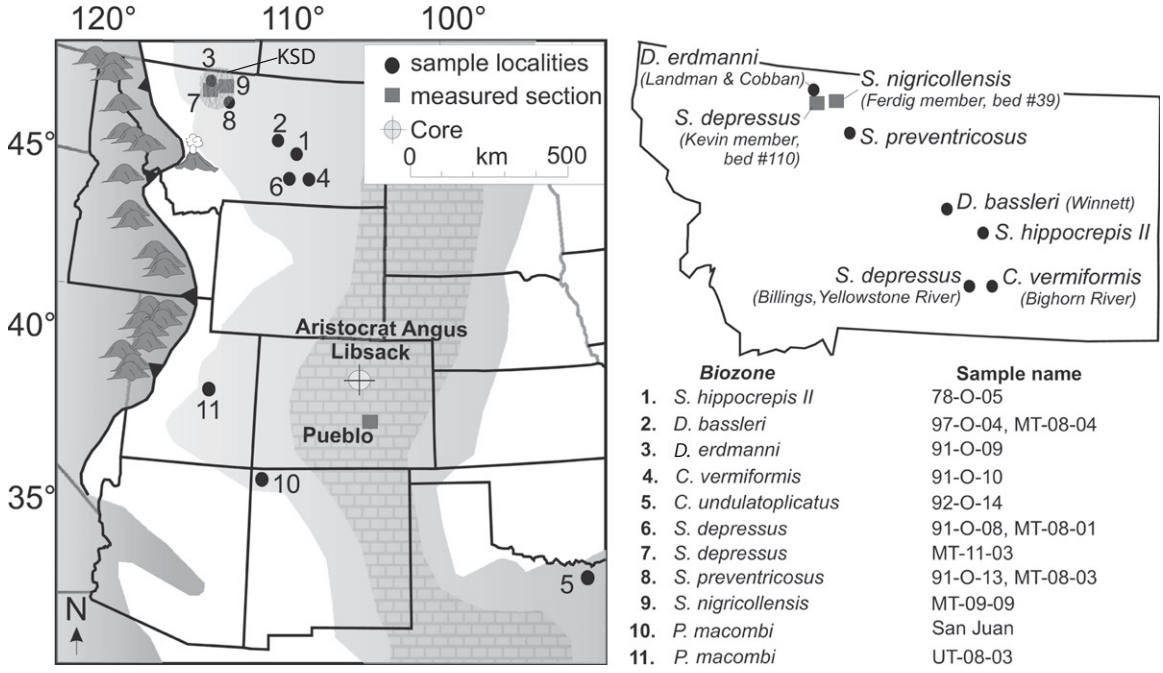

	Biozone	Sample name
1.	*S. hippocrepis II*	78-O-05
2.	*D. bassleri*	97-O-04, MT-08-04
3.	*D. erdmanni*	91-O-09
4.	*C. vermiformis*	91-O-10
5.	*C. undulatoplicatus*	92-O-14
6.	*S. depressus*	91-O-08, MT-08-01
7.	*S. depressus*	MT-11-03
8.	*S. preventricosus*	91-O-13, MT-08-03
9.	*S. nigricollensis*	MT-09-09
10.	*P. macombi*	San Juan
11.	*P. macombi*	UT-08-03

Figure 1. Regional map modified from Roberts and Kirschbaum (1995) indicating location of: (1) Montana sites (1–4, 6–9) where most ash beds analyzed in this study were sampled (ashes from two biozones were sampled elsewhere, at sites 5, 10, and 11); (2) Montana measured sections of the Kevin and Ferdig Members of the Marias River Shale (squares), based on Cobban et al. (1976); (3) Libsack and Aristocrat Angus boreholes in Colorado (circle with cross-hairs, representing location of both cores, drilled within 5 km of each other); and (4) measured section of the Niobrara Formation (square) near Pueblo, Colorado, based on Scott and Cobban (1964). The locality numbering scheme begins with the uppermost biozone and increases with age and stratigraphic depth; numbered ash layers were sampled within corresponding ammonite biozones, originally by Bill Cobban and colleagues (including Al Merewether and Neil Landman). Obradovich (1993) sample separates re-analyzed in this study begin with his sample numbers (e.g., 97-O-04), whereas new University of Wisconsin–Madison samples begin with state abbreviations (e.g., MT-08-04). KSD—Kevin-Sunburst Dome. See Table DR1.1 in the Data Repository [see footnote 1] for more detailed sample and locality information.

identification of key stratigraphic hiatuses that were not apparent in the long eccentricity–based time scale of Locklair and Sageman (2008). This leads to the third purpose of our research. In addition to the analytical uncertainties associated with radioisotopic age determinations, we introduce a new approach for assessing age uncertainty resulting from the correlation process. The integration of $^{40}Ar/^{39}Ar$, U-Pb, and astrochronologic age models in our revision of the Turonian-Coniacian, Coniacian-Santonian, and Santonian-Campanian stage boundaries accounts for uncertainty associated with $^{40}Ar/^{39}Ar$ geochronology, U-Pb geochronology, astrochronology, and the geologic components of uncertainty due to correlation, interpolation of stage boundary ages, and the presence of stratigraphic hiatuses.

STRATIGRAPHIC FRAMEWORK

The Niobrara Formation

Strata of the Niobrara Formation were originally documented by Meek and Hayden (1861) for exposures near the confluence of the Niobrara and Missouri Rivers in Nebraska and described as consisting of calcareous marl with chalk and limestone. The interval was later divided by Logan (1897) into lower Fort Hays Limestone and upper Smoky Hill Shale in western Kansas. A complicated history of stratigraphic terminology ensued until formal lithostratigraphic nomenclature was proposed by Scott and Cobban (1964). This history, integrating Niobrara research across Kansas and Colorado, is reviewed by Scott and Cobban (1964) and Hattin (1982) and has been illustrated in chart form by those authors (table 1 of each report).

According to Scott and Cobban (1964), the Niobrara Formation in Pueblo, Colorado, includes the two formal members defined in Kansas: the 12.1 m (40 ft)–thick basal Fort Hays Limestone Member and the overlying 213 m (700 ft)–thick Smoky Hill Chalk Member (Fig. 2). The Smoky Hill Chalk Member was further subdivided by Scott and Cobban (1964) into seven decameter-scale informal units including, from top to bottom: upper chalk, upper chalky shale, middle chalk, middle shale, lower limestone, lower shale, and lower shale and limestone (Fig. 2). The Scott and Cobban (1964) terminology for lithologic units of the Smoky Hill Member was modified by Dean and Arthur (1998) based on whole-rock major element carbonate content of samples from the Berthoud State #4 (and part of #3) cores. Dean and Arthur (1998) substituted the terms "marl" for "shale" or "chalky shale" and "chalk" for "limestone" (except in the lowermost unit, which they called lower chalk and shale) using a cutoff of 75 wt% $CaCO_3$ to separate chalk from marl units. Longman et al. (1998) also subdivided the Smoky Hill Member into marl and chalk units, with the boundary between marl and chalky marl/chalk lithologic components placed at 65 wt% $CaCO_3$. They also demonstrated the wide range of lithologic and thickness variability in the Niobrara Formation across an eight-state region. In Kansas and Nebraska, the entire thickness of the Niobrara may be classified as limestone or chalk, while in eastern Colorado, New Mexico, and Wyoming, the Smoky Hill consists of alternating chalk and marl. Further west in Colorado, Utah, and New Mexico, the entire Niobrara carbonate interval can be stratigraphically assigned to an informal calcareous shale member of the Mancos Shale. In this paper, the original Smoky Hill unit names of Scott and Cobban (1964) are used.

Biostratigraphy has played a critical role in the development of a chronostratigraphic framework for the Niobrara Formation and its time-equivalent strata in the Western Interior Basin. The ammonite biozonation scheme for the Niobrara interval, spanning the *Scaphites preventricosus* through *S. hippocrepis* III biozones, was developed based on fossil occurrence data keyed to bed numbers in the original Scott and Cobban (1964) measured section for Pueblo, augmented by data from many other Western Interior localities (summarized in Cobban, 1993; Cobban et al., 2006), and this scheme remains the standard for Coniacian-Santonian biostratigraphy in the Western Interior (Cobban et al., 2006). In addition, inoceramid bivalves are common and widespread in Coniacian-Santonian strata and their biozones have as much biostratigraphic utility as ammonites for this time period. As such, the recent work by Walaszczyk and Cobban (1999, 2000, 2007) provides an important complement to the ammonite biozonation, including inoceramid zones that are correlated to time-equivalent sections in Europe. Collectively, ~12 ammonite and 13 inoceramid biozones (Cobban et al., 2006) span the Niobrara study interval discussed in

Figure 2 (*on following page*). Biostratigraphic and lithostratigraphic correlation of the study interval from Montana (including Ferdig Member and Kevin Member of Marias River Shale, Telegraph Creek Formation, and Virgelle Sandstone or Eagle Sandstone) to the uppermost Carlile Formation and Niobrara Formation in the Pueblo, Colorado, area (outcrop) and the Denver Basin (Libsack 43-27 core; note Libsack scale change). Modified stratigraphic columns and fossil range data are sourced as follows: Montana—section A includes the upper part of Landman and Cobban's (2007) measured section; sections B and C represent the Kevin and Ferdig Member type sections, respectively, from Cobban et al. (1976); Pueblo—outcrop measured section from Scott and Cobban (1964) and Fisher et al. (1985) with updated fossil range data from Walaszczyk and Cobban (2000, 2006, 2007); Libsack core—measured section from Locklair (2007) and Locklair and Sageman (2008). Sampled ash beds are keyed to the locality map in Figure 1 with locality numbers, shown in columns that identify those from the Kevin-Sunburst Dome area (K-S dome, sections A–C), and those from other sites in Montana (arrows indicate they are projected into the K-S dome sections based on biostratigraphy). Biozone boundaries in the Kevin and Pueblo sections are determined by fossil occurrence data, labeled adjacent to the sections. Where index taxa are scarce (uppermost Santonian to Campanian in Pueblo), biozone boundaries are estimated and their projection to the Libsack core is shown with a query. Further detail on biostratigraphic assignments, ash correlations, and locality data are presented in the Data Repository [see footnote 1]. Abbreviations for Niobrara lithostratigraphic units are: upper chalk (UC), upper chalky shale (UCS), middle chalk (MC), middle shale (MS), lower limestone (LL), lower shale (LS), lower shale and limestone (LSL), and Fort Hays Limestone (FHLS). SS—sandstone; carb/phos—carbonate/phosphatic; LAD—Last Appearance Datum; FAD—First Appearance Datum. *Ammonites: Prionocyclus hyatti*, *Prionocyclus macombi*, *Scaphites warreni*, *Scaphites nigricollensis*, *Scaphites preventricosus, Scaphites ventricosus*, *Scaphites depressus*, *Clioscaphites saxitonianus*, *Clioscaphites vermiformis*, *Clioscaphites choteauensis*, *Desmoscaphites erdmanni*, *Desmoscaphites bassleri*, *Haresciceras mancosense*, *Haresciceras montanaense*, *Scaphites leei* III, *Scaphites hippocrepis* I, *Scaphites hippocrepis* II, *Haresiceras placentiforme*, *Haresiceras natronense*. *Inoceramids: Cremnoceramus erectus*, *Magadiceramus subquadratus*, *Cremnoceramus waltersdorfensis*, *Cremnoceramus waltersdorfensis hannoverensis*, *Cremnoceramus crassus inconstans*, *Volviceramus koeneni*, *Volviceramus involutus*, *"Inoceramus" gibbosus*, *Cladoceramus undulatoplicatus*, *Cordiceramus muelleri*, *Platyceramus platinus*.

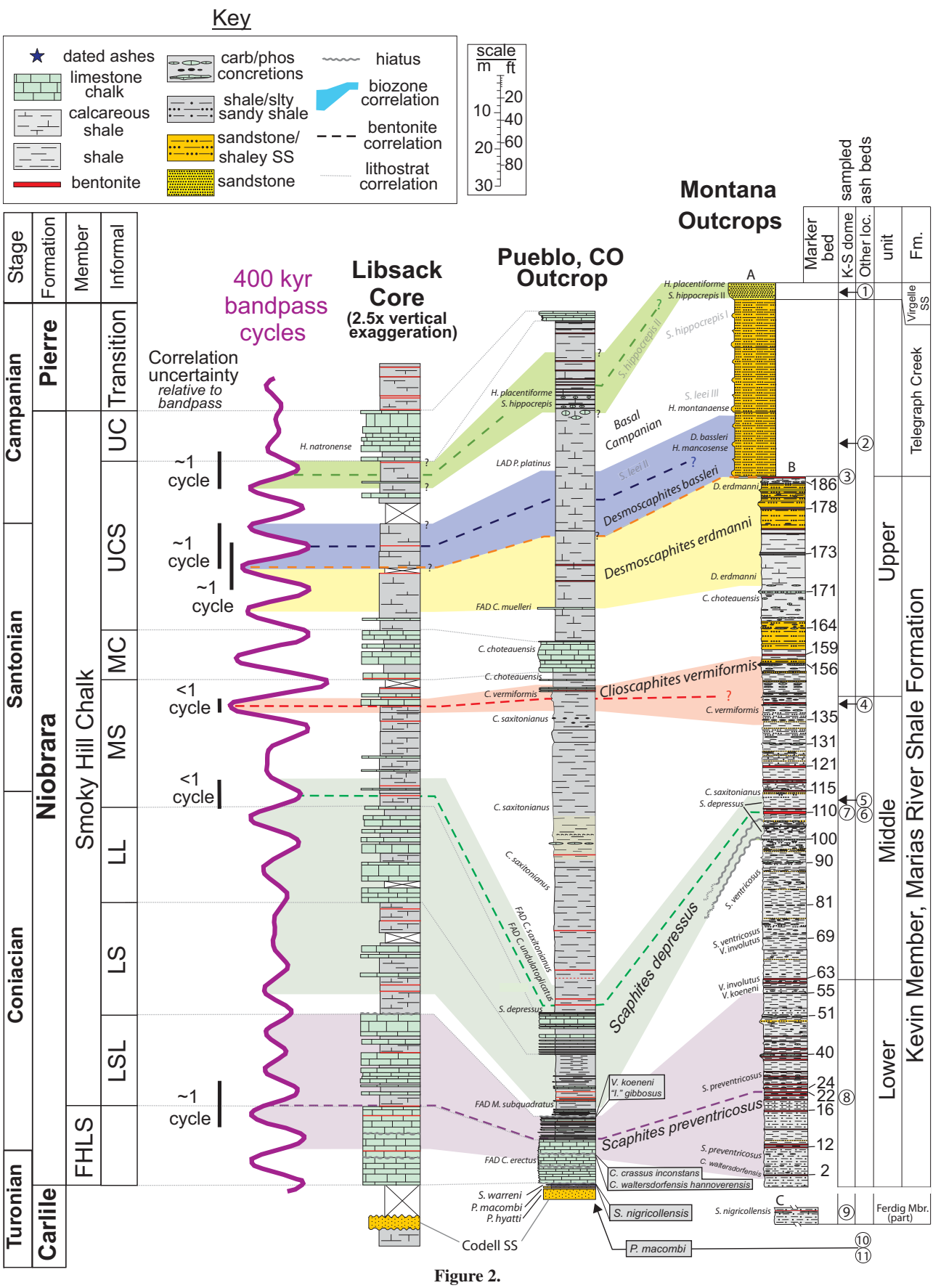

Figure 2.

this paper and these zones have been previously calibrated to the geologic time scale, mostly based on Obradovich (1993) and Cobban et al. (2006) (e.g., Ogg et al., 2004; Ogg and Hinnov, 2012). Selected index taxa shown in Figure 2 constrain the assignment of biozone boundaries. In the Pueblo section, fossil data for the upper Carlile Formation come from Fisher et al. (1985) and the Niobrara sources are Scott and Cobban (1964) and Walaszczyk and Cobban (1999, 2000, 2006). Detailed explanations for all biostratigraphic assignments and stratigraphic correlations are provided in an Appendix DR2 in the GSA Data Repository[1].

The Niobrara Formation also preserves centimeter- to decimeter-scale rhythmic lithologic alternations between carbonate-rich layers and more clay- and organic matter–rich layers that have been interpreted to reflect orbital influence on sedimentation (Gilbert, 1895; Fischer et al., 1985; Savrda and Bottjer, 1989; Arthur and Dean, 1991; Fischer, 1993; Pratt et al., 1993; Ricken, 1994; Dean and Arthur, 1998; Locklair and Sageman, 2008). These so-called Milankovitch cycles offer an additional chronostratigraphic tool for the quantification of Niobrara time. An estimate of total Niobrara duration based on the cyclostratigraphy of Locklair and Sageman (2008) yields values ranging from 6.1–7.2 m.y. This estimate seemed plausible based on the $^{40}Ar/^{39}Ar$ geochronology of Obradovich (1993), which allows values ranging from 6.5 to 8.6 m.y. for total duration when analytical uncertainties and interpolation from ash horizons to formation boundaries are considered. In this study, the significance of new radioisotopic data and additional geologic observations are evaluated.

The Niobrara Formation is 225.6 m (740 ft) thick in Scott and Cobban's (1964) Pueblo measured section of outcrop, but generally thinner in cored sections such as those from the Denver Basin (e.g., 84.5 m = 277 ft in Encana Libsack 43-27 well [API {American Petroleum Institute}well number 05-123-21838, sec. 27, tp. 4N, rge. 65W {40°16′54.86″N, 104°38′32.17″W}]) where an astrochronologic analysis was performed by Locklair and Sageman (2008). Despite thickness changes, the characteristic lithologic units of the Niobrara Formation, described above, can be recognized and traced over large areas (e.g., Longman et al., 1998), including between Pueblo and the Denver Basin where bentonites and limestone/chalk beds are the basis for the lithostratigraphic correlation (Locklair, 2007).

Correlation of Marias River Shale, Telegraph Creek Formation, and Virgelle/Eagle Sandstone to the Niobrara Formation

Based on biostratigraphy (Cobban, 1964; Cobban et al., 1976, 2005; Landman and Cobban, 2007), strata of the Marias River Shale, Telegraph Creek Formation, and Virgelle/Eagle Sandstones in Montana are time equivalent to the Turonian through lowermost Campanian interval shown in Figure 2. These strata contain a succession of ash beds preserving datable minerals and were the focus of Obradovich's (1993) $^{40}Ar/^{39}Ar$ age determinations for the latest Turonian through early Campanian. The sections shown in Figure 2 represent a Montana composite because some ash beds had to be sampled in other Montana localities and projected into the composite using biostratigraphy (Appendix DR2). This composite includes three sections from the Kevin-Sunburst Dome area (Cobban et al., 1976).

The lowermost sampled ash bed is associated with fossils of *S. nigricollensis*, representing a late Turonian biozone that correlates to an unconformity at the base of the Niobrara Formation at Pueblo. It was sampled in the Ferdig Member of the Marias River Shale. The Ferdig Member consists of gray noncalcareous shales with thin sandy laminae and carbonate concretions and contains several ash horizons. The sample locality was near the Ferdig type section of Cobban et al. (1976) and is represented by a partial section labeled C in Figure 2 (Appendix DR2). This ash provides a lower age constraint for the study interval. The Turonian-Coniacian boundary occurs a few meters above this level in Pueblo and is defined by the FAD (First Appearance Datum) of *Cremnoceramus erectus*, which also constrains the lower boundary of the *S. preventricosus* biozone (Walaszczyk and Cobban, 2006).

The main part of the succession, segment B of the Montana stratigraphic column in Figure 2 (loc. 7, Fig. 1), includes the Kevin Member of the Marias River Shale and is the Kevin type section of Cobban et al. (1976). The Kevin Member consists of gray marine shales interbedded with thin sandy layers, calcareous concretions, and numerous bentonitic marker beds and is subdivided into lower, middle, and upper units on the basis of the ash bed abundance and concretion types, originally described by Erdmann et al. (1947). Fossil range data documented by Cobban et al. (1976, 2005), Landman and Cobban (2007), and Grifi et al. (2013) allow the following designations: The lower unit contains *S. preventricosus* and is correlative with the Fort Hays Limestone Member and lower shale and limestone (LSL) unit of the Smoky Hill Chalk Member in Pueblo (Fig. 2). The middle unit contains index taxa representing the *Scaphites ventricosus*, *Scaphites depressus*, *Clioscaphites saxitonianus*, and *Clioscaphites vermiformis* biozones and is equivalent to the lower shale (LS) through middle shale (MS) units of the Smoky Hill Chalk Member in Pueblo (Fig. 2). The Coniacian-Santonian boundary occurs within this interval, constrained in the Pueblo section by the FAD of *Cladoceramus undulatoplicatus*, which is overlain by the FAD of *C. saxitonianus* marking the top of the *S. depressus* biozone (Walaszczyk and Cobban, 2006) (Fig. 2). The close succession of *S. depressus* and *C. saxitonianus* in the Kevin section fix the position of the Coniacian-Santonian boundary in Montana (Fig. 2). The upper unit of the Kevin Member contains the *C. vermiformis*, *Clioscaphites choteauensis*, and *Desmoscaphites erdmanni* biozones and is time correlative with the top of the middle shale (MS) through part of the upper chalky shale (UCS) of the Smoky Hill Chalk in Pueblo (Fig. 2).

The Telegraph Creek Formation overlies the Kevin Member and consists of sandy shale, siltstone, and thin shaley sandstone beds (Landman and Cobban, 2007). In the Marias River section of Landman and Cobban (2007), represented by section A in Figure 2, the Telegraph Creek is overlain by part of the Virgelle Sandstone. This sand unit is part of a time-transgressive clastic wedge that grades to younger facies of the Eagle Sandstone toward the southeast (Cobban, 1964). According to Cobban (1964), Cobban (1969), and Landman and Cobban (2007), the Telegraph Creek in the Marias River section contains *Desmoscaphites bassleri* and *Haresiceras mancosense* followed upsection by *Haresiceras montanense* (equivalent to *Scaphites leei* III), and the Eagle Sandstone contains *Haresiceras placentiforme* and *Scaphites hippocrepis* II overlain by *Scaphites hippocrepis* III and *Haresiceras natronense*. Ash beds were sampled in strata containing *D. bassleri* and *S. hippocrepis* II (see Appendix DR2); the latter provides age constraint near the top of the Niobrara study interval. Collectively, these taxa facilitate correlation of the Telegraph Creek and Virgelle/Eagle Sandstones to the upper chalky shale through upper chalk of the Smoky Hill Member in Pueblo. The Santonian-Campanian boundary occurs within this interval, defined at the base of the *S. leei* III biozone (top of *D. bassleri*), and just below the LAD (Last Appearance Datum) of *Platyceramus platinus* (as referred to by

[1]GSA Data Repository item 2014122, (1) Detailed information on sample locations and descriptions; (2) An appendix of biostratigraphic data for the study; (3) Detailed data pertaining to the U-Pb zircon geochronology; (4) Detailed data pertaining to the $^{40}Ar/^{39}Ar$ sanidine geochronology; and (5) References specific to the supplement, is available at http://www.geosociety.org/pubs/ft2014.htm or by request to editing@geosociety.org.

Scott and Cobban, 1964) which is used to define the upper boundary of the *D. bassleri* zone in Pueblo (Fig. 2).

PREVIOUS GEOCHRONOLOGIC STUDIES

Radioisotopic Geochronology

Using the $^{40}Ar/^{39}Ar$ technique and a U.S. Geological Survey (USGS) internal standard sanidine from the Taylor Creek Rhyolite, and assuming its age to be 28.32 Ma—essentially equivalent to a FCs standard age of 28.02 Ma—Obradovich (1993) analyzed sanidine crystals from 29 Western Interior Basin ash beds. Six of these bentonites fall within the ~10 m.y. interval that is the focus of the present study (*P. macombi* through *S. hippocrepis* II ammonite zones) and the ages produced from these ashes have analytical uncertainties ranging between ±0.28 and ±0.72 m.y. (95% confidence level, analytical uncertainties only; Table 1). Agterberg (1994) fit a cubic spline to these $^{40}Ar/^{39}Ar$ ages to extrapolate six Late Cretaceous stage boundaries and their associated uncertainties. In the 2004 International Geologic Time Scale, Ogg et al. (2004, 2008; GTS2004) refined this spline curve to extrapolate ages of 88.8 ± 1.0 Ma for the base of the Coniacian, 85.8 ± 0.7 Ma for the base of the Santonian, and 83.5 ± 0.7 Ma for the base of the Campanian. The uncertainties on Late Cretaceous stage boundaries in the GTS2004 are ~1% but underestimate the external sources of uncertainty associated with the $^{40}Ar/^{39}Ar$ technique (Ogg et al., 2004). Since the publication of GTS2004 and the short update in 2008 there have been significant advances in both the $^{40}Ar/^{39}Ar$ and U-Pb methods that have been adopted by Gradstein et al. (2012) in the 2012 International Geologic Time Scale (GTS2012). Key innovations of GTS2012 (Schmitz, 2012) are: (1) adoption by the majority in the $^{40}Ar/^{39}Ar$ community of the astronomically calibrated age of the FCs standard of 28.201 ± 0.046 Ma and the preferred ^{40}K decay constant of $5.463 \pm 0.107 \times 10^{-10}$ (Kuiper et al., 2008; Min et al., 2000); and (2) the use of U-Pb isotope data mainly from zircons that have been measured using the chemical abrasion–isotope dilution–thermal ionization mass spectrometry(CA-ID-TIMS) method (Mattinson, 2005), EARTHTIME (http://www.earth-time.org/) tracer solutions that have been cross-calibrated in several U-Pb laboratories, and the uranium decay constant ratio of Mattinson (2010). Adoption of the Kuiper et al. (2008) standardization of the $^{40}Ar/^{39}Ar$ method allows age determinations with total uncertainties (analytical + standard + decay constant) of as good as ±0.3%, whereas modern CA-ID-TIMS U-Pb ages can have total uncertainties <0.2% (Schmitz, 2012) due to fully traceable calibration of the U-Pb system. Thus, the total uncertainty on the ages of salient Late Cretaceous ash beds reported here and in Meyers et al. (2012) is better than one-half of a 405 k.y. eccentricity cycle, thereby providing $^{40}Ar/^{39}Ar$ and U-Pb tie points that are sufficiently precise to calibrate floating astrochronologic age models.

The framework of our $^{40}Ar/^{39}Ar$ and U-Pb isotopic data sets was reported in the unpublished Master of Science thesis of Siewert (2011) and these ages were used in GTS2012 by Ogg and Hinnov (2012) to constrain the ages of the Turonian-Coniacian, Coniacian-Santonian, and Santonian-Campanian stage boundaries at 89.8 ± 0.4, 86.3 ± 0.5, and 83.6 ± 0.3 Ma, respectively. In addition to the radioisotopic data of Siewert (2011), this paper reports the $^{40}Ar/^{39}Ar$ age of a key ash bed from the Kevin Member of the Marias River Shale in the *S. depressus* ammonite zone, as well as new biostratigraphic information that bears on an accurate correlation of the ash beds between outcrops and drilled cores from which the astrochronology derives. The stage boundary ages reported here reflect these improvements.

Basis of the Astronomical Time Scale

Gilbert (1895) first proposed that the chalk-marl sequences of the Niobrara Formation reflect a climatic response due to orbital forcing from which a duration of geologic time might be estimated. This concept was later summarized and further explored by Fischer (1980), Fischer et al. (1985), and Fischer and Bottjer (1991). Locklair and Sageman (2008) developed a quantitative ATS for the Niobrara Formation based on two sections preserved within the Libsack 43-27 and Aristocrat Angus 12-8 boreholes, drilled in the Wattenberg field on the west side of the Denver Basin (Fig. 1). Using advanced spectral analytical techniques, such as multi-taper method spectral analysis (Thomson, 1982), bandpass-filter analyses (Gaussian), and evolutive harmonic analysis (Meyers et al., 2001) on micro-resistivity images that can resolve bedding features at the centimeter scale, Locklair and Sageman (2008) identified several astronomical signals related to eccentricity, obliquity, and precession. This study builds on the results of Locklair and Sageman (2008) to revise stage boundary ages through interpolation of radioisotopic ages with the ATS based on 405 k.y. eccentricity cycles that are expressed in the periodic meter-scale variation of the Niobrara lithologic record (Locklair and Sageman, 2008).

METHODOLOGY

Sample Descriptions

Western Interior Basin ash beds are commonly subtly graded, thus most were sampled from the base to maximize phenocryst content and grain size. The majority of dated units are preserved within vertically extensive shale beds, which limits contamination by detrital grains. Ash beds were primarily sampled in Montana (biozones 1–4, 6–9, Fig. 1), while the *Cladoceramus undulatoplicatus* (an inoceramid corresponding to the upper part of the *S. depressus* zone) ash was sampled in Texas, and *P. macombi* ashes were sampled in Utah and New Mexico (Figs. 1–2, Table 1; see also Table DR1.1 and Figure DR1.2 for complete bentonite descriptions and locations). If a bentonite was sampled above or below the orbitally tuned strata, or if we could not be certain of the location of the bentonite within a formation or biozone (e.g., the *C. undulatoplicatus* ash from the Austin Chalk, Texas), it is not correlated into the Libsack core and used to evaluate stage boundary ages. $^{40}Ar/^{39}Ar$ ages from *C. undulatoplicatus*, *C. vermiformis*, *D. erdmanni*, and *S. hippocrepis* II biozones are based solely on new $^{40}Ar/^{39}Ar$ data acquired from Obradovich (1993) legacy samples; although Obradovich separated sanidines from these samples, he did not previously determine ages in the *C. vermiformis* and *D. erdmanni* biozones. For six of the ammonite biozones, we have both an $^{40}Ar/^{39}Ar$ age from a newly collected University of Wisconsin–Madison sample and an Obradovich (1993) legacy sample. Four ammonite biozones—*P. macombi*, *S. preventricosus*, *S. depressus*, and *D. bassleri*—have paired $^{206}Pb/^{238}U$ and $^{40}Ar/^{39}Ar$ data obtained from newly collected samples. Moreover, we now have two distinct $^{40}Ar/^{39}Ar$ ages from ash beds in Montana within the *S. depressus* zone.

U-Pb Geochronology

Zircons were separated from multi-kilogram bentonite samples following methods outlined in Meyers et al. (2012) and imaged using backscatter electron and cathodoluminescence (CL) mode on a Hitachi S3400-N scanning electron microprobe (SEM) at the University of Wisconsin–Madison. Single zircons or fragments of zircons were selected based on external morphology and internal growth zonation revealed by cathodoluminescence imaging (Fig. DR2.2). Prior to complete dissolution, zircons were chemically annealed and partially dissolved to preferentially remove radiation-damaged areas within the crystal lattice (Mattinson, 2005). Solutions were spiked with the ET535 tracer

TABLE 1. SUMMARY OF $^{40}Ar/^{39}Ar$ AND $^{206}Pb/^{238}U$ AGES

Biozone Sample	Obradovich (1993)*		University of Wisconsin–Madison $^{40}Ar/^{39}Ar$ fusion analyses												NIGL $^{206}Pb/^{238}U$ isotope analyses				
						Apparent ages			Apparent ages			Apparent ages							
	TCs 28.32 Ma†					FCs 28.02 Ma§			FCs 28.294 Ma#			FCs 28.201 Ma**							
	Age (Ma)	±95%††	Aliquot size	N	MSWD	Age (Ma)	±2σ††	±2σ§§	Age (Ma)	±2σ††	±2σ##	Age (Ma)	±2σ††	±2σ§§	N	MSWD	Age (Ma)	±2σ††	±2σ§§
***Scaphites hippocrepis* II**																			
78-O-05	81.71	±0.34	1	16 of 16	0.65	81.22	±0.21	±0.54	82.01	±0.21	±0.22	81.78	±0.21	±0.34					
78-O-05	81.71	±0.34	3	27 of 28	0.97	81.32	±0.14	±0.54	82.12	±0.14	±0.15	81.87	±0.14	±0.31					
			weighted mean:	2		81.27	±0.11	±0.38	82.08	±0.11	±0.12	**81.84**	**±0.11**	**±0.22**					
Desmoscaphites bassleri																			
MT-08-04			3 to 4	32 of 36	0.37	83.81	±0.19	±0.56	84.63	±0.20	±0.20	84.38	±0.19	±0.34	4 of 17	1.5	**84.43**	**±0.09**	**±0.15**
97-O-04	83.91	±0.43	4	32 of 34	0.68	83.87	±0.22	±0.56	84.69	±0.22	±0.22	84.44	±0.22	±0.36					
			weighted mean:	2		83.84	±0.14	±0.39	84.65	±0.14	±0.15	**84.41**	**±0.14**	**±0.24**					
Desmoscaphites erdmanni																			
91-O-09			5 to 7	22 of 36	1.00	83.98	±0.24	±0.56	84.79	±0.24	±0.25	**84.55**	**±0.24**	**±0.37**					
Clioscaphites vermiformis																			
90-O-10			7	11 of 11	0.97	84.95	±0.24	±0.57	85.78	±0.25	±0.25	85.53	±0.25	±0.38					
90-O-10			10	28 of 34	0.94	85.16	±0.14	±0.57	85.99	±0.14	±0.15	85.74	±0.14	±0.32					
90-O-10(i)			>10	6 of 6	0.69	85.04	±0.14	±0.57	85.87	±0.14	±0.15	85.62	±0.14	±0.32					
			weighted mean:	3		85.05	±0.09	±0.32	85.91	±0.09	±0.10	**85.66**	**±0.09**	**±0.19**					
Cladoceramus undulatoplicatus																			
92-O-14	84.88	±0.28	5	19 of 25	0.86	85.26	±0.24	±0.57	86.08	±0.24	±0.25	**85.84**	**±0.24**	**±0.37**					
Scaphites depressus																			
MT-11-03			4	25 of 25	0.99	85.96	±0.12	±0.58	86.79	±0.12	±0.13	**86.52**	**±0.12**	**±0.33**					
MT-08-01			5	20 of 32	0.31	86.53	±0.20	±0.58	87.37	±0.20	±0.21	87.12	±0.20	±0.36	7 of 11	1.8	**87.11**	**±0.08**	**±0.15**
MT-08-01			5	28 of 43	0.65	86.53	±0.14	±0.58	87.37	±0.14	±0.15	87.12	±0.14	±0.32					
91-O-08	86.92	±0.39	4	26 of 27	0.43	86.55	±0.13	±0.58	87.39	±0.13	±0.14	87.14	±0.13	±0.32					
			weighted mean:	3		86.54	±0.08	±0.33	87.38	±0.09	±0.09	**87.13**	**±0.09**	**±0.19**					
Scaphites preventricosus																			
91-O-13	88.34	±0.60	10	43 of 44	0.83	88.64	±0.19	±0.59	89.50	±0.19	±0.19	89.24	±0.19	±0.35					
MT-08-03			1	26 of 40	0.96	88.75	±0.14	±0.59	89.61	±0.14	±0.15	89.36	±0.14	±0.33	4 of 18	2.3	**89.37**	**±0.07**	**±0.15**
				2		88.69	±0.11	±0.41	89.57	±0.11	±0.12	**89.32**	**±0.11**	**±0.24**					
Scaphites nigricollensis																			
MT-09-09			8	50 of 55	0.86	89.22	±0.14	±0.60	90.09	±0.15	±0.16	89.83	±0.14	±0.25					
MT-09-09(i)			>10	8 of 8	0.97	89.30	±0.15	±0.60	90.17	±0.15	±0.16	89.91	±0.15	±0.25					
			weighted mean:	2		89.26	±0.10	±0.41	90.13	±0.10	±0.11	**89.87**	**±0.10**	**±0.18**					
***Prionocyclus macombi* (upper and lower ash beds?)**																			
UT-08-03			1	41 of 45	1.19	90.56	±0.13	±0.61	91.45	±0.13	±0.14	91.18	±0.13	±0.33	5 of 11	1.3	**91.37**	**±0.08**	**±0.15**
SAN JUAN	90.21	±0.72	10	44 of 48	1.03	90.67	±0.12	±0.61	91.55	±0.12	±0.13	91.29	±0.12	±0.33					
				2		90.61	±0.09	±0.42	91.50	±0.09	±0.10	**91.24**	**±0.09**	**±0.23**					

Note: Summary of 593 individual analyses (579 laser fusion, and 2 incremental heating experiments). Samples were correlated with biozones using Cobban et al. (2006). Weighted mean ages for Ar-Ar and U-Pb systems were determined using Isoplot 3.71 (Ludwig, 2003). $^{206}Pb/^{238}U$ ages are relative to Jaffey et al. (1971) decay constants and were spiked with the ET535 tracer solution. NIGL—National Environment Research Council Isotope Geosciences Laboratory; MSWD—mean square of weighted deviates.

*Re-dated legacy samples include ages from Obradovich (1993).

†Ages relative to 28.32 Ma Taylor Creek sanidine (TCs) (Duffield and Dalrymple, 1990) using Steiger and Jäger (1977) decay constant.

§Ages relative to 28.02 Ma Fish Canyon sanidine (FCs) (Renne et al., 1998) using Steiger and Jäger (1977) decay constant.

#Monte Carlo ages relative to 28.294 Ma FCs and decay constant in Renne et al. (2011).

**Ages relative to 28.201 Ma for FCs (Kuiper et al., 2008) using Min et al. (2000) decay constant.

††Analytical uncertainty at the 95% confidence level including J uncertainty.

§§Fully propagated uncertainty ($^{206}Pb/^{238}U$ includes decay constant, tracer solution, analytical uncertainties; $^{40}Ar/^{39}Ar$ includes uncertainties associated with the decay constants and the analyses themselves, the latter incorporating uncertainty in the age of the FCs standard minerals through measurement of the J value). For $^{40}Ar/^{39}Ar$ ages calculated relative to 28.02 Ma FCs, total uncertainty is estimated at 0.7% based on data from the Laschamp excursion (Guillou et al., 2004; Singer et al., 2009).

##Fully propagated uncertainty $^{40}Ar/^{39}Ar$ includes decay constant and analytical uncertainties using Monte Carlo simulations. i—incremental heating experiments.

solution (Condon et al., 2007) and analyzed at the Natural Environment Research Council Isotope Geosciences Laboratory (NIGL) on a Thermo-Electron Triton TIMS instrument. These CA-ID-TIMS procedures follow those of Meyers et al. (2012). More information on these procedures is in Appendix DR3.1 and the complete U-Pb isotope data are in Table DR3.3.

$^{40}Ar/^{39}Ar$ Geochronology

Approximately 9 kg of bulk material from each of the ash beds was processed for sanidine using techniques outlined in Meyers et al. (2012). The purity of the sanidine separates and those from Obradovich (1993) legacy samples were assessed using an SEM equipped with an energy-dispersive X-ray spectrometer detector such that single sanidine crystals were isolated from quartz and plagioclase phenocrysts. FCs crystals were used as the primary neutron fluence monitor. At the University of Wisconsin–Madison Rare Gas Geochronology Laboratory, sanidine samples and standards were fused using a 25 W CO_2 laser following the methods of Smith et al. (2008) and Meyers et al. (2012). Analysis of peak signal data collected on a MAP 215-50 mass spectrometer using a single electron multiplier was done using ArArCalc 2.5 (http://earthref.org/ArArCALC/), but differs slightly from the approach taken in our prior work. The procedure for peak signal regression and filtering of outliers reduces the analytical uncertainty associated with each age determination by ~15%–20% compared to our previous studies (Smith et al., 2010; Meyers et al., 2012) and is fully explained in Appendix DR4.1.

The analytical uncertainty of each individual $^{40}Ar/^{39}Ar$ fusion age is reported at the 2σ level. Weighted mean ages incorporate an MSWD (mean square of weighted deviates) criterion to estimate the 95% confidence interval from observed scatter (see Ludwig, 2003, for details). Total radioisotopic uncertainties (analytical + standard mineral age + decay constants) are reported at the 2σ level. For the $^{40}Ar/^{39}Ar$ ages calculated relative to FCs at 28.201 Ma these are determined following equation 5 of Renne et al. (1998). In contrast, the $^{40}Ar/^{39}Ar$ ages calculated relative to a FCs age of 28.294 Ma (Renne et al., 2011) utilize Monte Carlo simulation to estimate the 95% confidence interval. The total uncertainty for ages calculated relative to an FCs age of 28.02 Ma is discussed below.

Uncertainty Associated with Integration of Radioisotopic and Astrochronologic Data

To anchor the ATS and interpolate stage boundary ages using the stable long eccentricity cycle the ages of radioisotopically dated bentonites collected in Montana must be projected into the stratigraphy of the orbitally tuned cores from the Denver Basin. This is accomplished using biostratigraphic and lithostratigraphic correlation. Specifically, FAD data for ammonite and inoceramid index taxa are used to determine the upper and lower boundaries of ammonite biozones in the Montana and Pueblo sections (see Appendix DR2). The Pueblo section, in turn, is correlated to the Libsack core record using lithostratigraphy (Fig. 2) because the latter lacks fossil data. Lithostratigraphic markers such as limestone/chalk beds and bentonites are tracked in relation to Niobrara lithostratigraphic units (which are clearly traceable along the Front Range in Colorado; Locklair, 2007), and these correlations are used to project biozone boundaries and ash horizons from Pueblo to the Libsack core. There are several potential sources of uncertainty in this correlation process, discussed below.

Ashes sampled in the Marias River Shale, Telegraph Creek Formation, or Eagle Sandstone in Montana are associated with zonal index taxa that allow each to be constrained to a specific ammonite biozone (see Appendix DR2). Each of these biozones is represented in the Pueblo section and can be projected into the Libsack core (Fig. 2). The major source of uncertainty in this correlation occurs when the relative position of a sampled ash within the biozone in Montana is not known (e.g., some of the best ash beds for dating can be associated with corresponding index taxa, but outcrop exposures do not allow upper and lower boundaries of the biozone to be determined). To accommodate the "correlation uncertainty" that this creates (as opposed to analytical or other types of uncertainty), such ash horizons are positioned in the center of the biozone and an uncertainty of ±0.5 of the biozone duration is added directly to the radioisotopic age of the ash (reflecting the fact that the ash horizon could fall anywhere within the biozone boundaries). In cases where the ash bed is stratigraphically well constrained within a biozone, or coincides with a biozone boundary, a smaller uncertainty can be applied. Each uncertainty estimate is determined based on the specific lithostratigraphic constraint of a given ash bed correlation (see below) and, because they are not normally distributed as are radioisotopic dating uncertainties that can be summed in quadrature, these are simply added to the sum of other uncertainties for each dated ash bed.

Additional sources of uncertainty derive from (1) the placement of biozone boundaries in the Pueblo section due to scarcity of key fossil taxa in some intervals; (2) the projection of biozones to the Libsack core, and thus to the long eccentricity bandpass used to determine biozone durations; (3) the correlation of bentonite beds, some of which are observed to vanish and reappear in correlated stratigraphic sections spanning significant distance (which means that, in the absence of additional chemical, mineralogical, or radioisotope data supporting a definitive correlation, e.g., Kowallis et al. [1989], most correlations are hypotheses); and (4) the presence of hiatuses in the section. The degree to which these uncertainties impact a given ash correlation and the associated determination of stage boundary ages is variable, however, and therefore sources of uncertainty are summarized for each ash individually (see below, Fig. 2, and Table 2).

TABLE 2. ASSESSMENT OF THE GEOLOGIC UNCERTAINTY ASSOCIATED WITH CORRELATING EACH ASH BED INTO THE ORBITALLY TUNED STRATIGRAPHY

Ammonite zone	Number of cycles (405 k.y. eccentricity)	Equivalent duration (k.y.)	Estimated uncertainty (k.y.)
Desmoscaphites bassleri	1.00	400	±200
Desmoscaphites erdmanni	1.00	400	±200
Clioscaphites vermiformis	0.35	140	±70
Scaphites depressus	0.50	200	±100
Scaphites preventricosus	1.00	400	±200

RESULTS

U-Pb Results

The U and Pb isotope composition of 7–13 single crystal or zircon fragments were analyzed from four ash beds that span the Niobrara Formation (Table 1; Fig. 3). In addition to examination of external crystal morphology, CL imaging was used in order to further guide our selection of zircon crystals/fragments for CA-ID-TIMS analyses. In general we avoided zircons with obvious internal zonation or discontinuities suggesting punctuated crystallization. For four crystals we were able to identify and subsample rim and core domains (Fig. DR3.2 and Table DR3.3) and inform subsequent sampling strategies. These core-rim pairs indicate a resolvable difference of ~300 k.y. for three of the four crystals. Advances in high-precision ID-TIMS U-Pb geochronology (reduced procedural blanks, increased ionization efficiency, improved ion counting systems, and perhaps

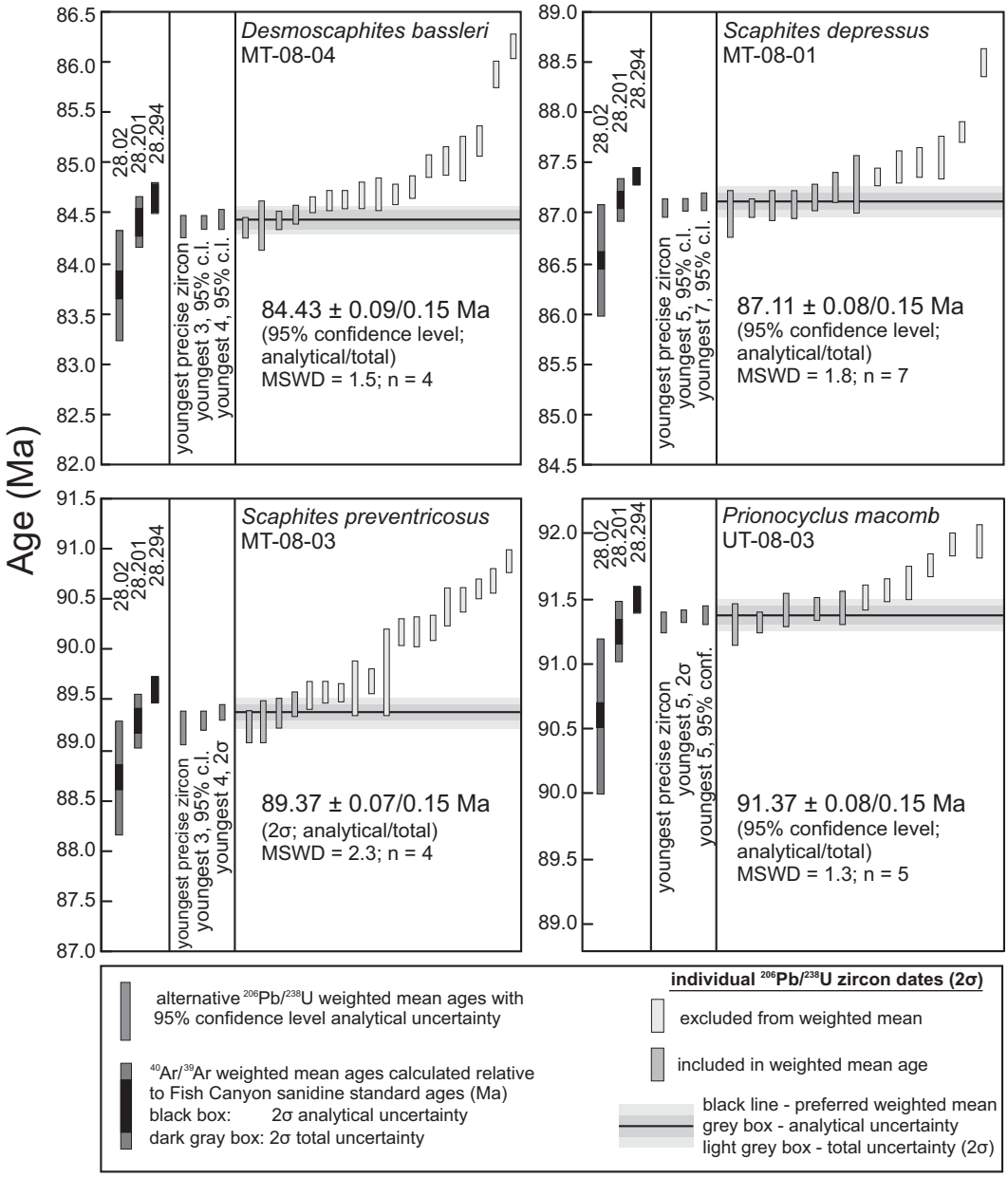

Figure 3. Ranked $^{206}Pb/^{238}U$ dates of single crystals or fragments of zircon from four ash beds (MSWD—mean square of weighted deviates). Individual analyses are shown with 2σ uncertainties; analyses in dark gray rectangles are included in the weighted mean age. Concordia plots of these data are in Figure DR3.7 in the Data Repository [see footnote 1]. Alternative weighted mean ages based on groupings of the youngest $^{206}Pb/^{238}U$ dates are explained in Figure DR3.6. For comparison, $^{40}Ar/^{39}Ar$ ages calculated using three pertinent ages for the Fish Canyon sanidine standard are shown to the left of the $^{206}Pb/^{238}U$ ages (see text for discussion).

most importantly, the effective elimination of Pb loss using the "chemical abrasion" method of Mattinson, 2005), have improved analytical uncertainties to <0.1% for an individual zircon crystal or fragment, thereby allowing the differentiation of juvenile magmatic zircons from those which may reflect xenocrystic or antecrystic components. U-Pb data from zircons in each ash bed reveal a significant spread in crystallization dates. Recent U-Pb zircon studies of both granitoid plutons (e.g., Miller et al., 2007; Schaltegger et al., 2009) as well as distal ash beds (e.g., Schoene et al., 2010; Meyers et al., 2012; Wotzlaw et al., 2013) have revealed similar ranges of zircon dates that reflect protracted zircon crystallization histories. Thus, some degree of interpretation is required to determine an eruption age from a suite of zircon dates that may span several hundred thousand years (Wotzlaw et al., 2013; Schoene et al., 2013).

For each sample we identify the population of youngest concordant zircons and calculate a $^{206}Pb/^{238}U$ weighted mean age as an approximation for the eruption age of the ash layer (Table 1; Fig. 3; see also Figure DR3.7). In each case the mean age is based on four to seven individual $^{206}Pb/^{238}U$ dates that include the youngest in each sample. The coherence of the youngest population is assessed via the MSWD value, each of which is within the acceptable range for the given number of analyses (Wendt and Carl, 1991). However, we recognize that there are multiple ways to interpret the distribution of $^{206}Pb/^{238}U$ dates from an ash bed, thus we outline alternative $^{206}Pb/^{238}U$ ages in Figure DR3.6. These alternative interpretations, for example using only the youngest zircon $^{206}Pb/^{238}U$ date as the best approximation of the youngest zircon in the ash bed, and inferentially the eruption age (e.g., Schoene et al., 2010; Wotzlaw et al., 2013), have minimal impact upon the standardization of the $^{40}Ar/^{39}Ar$ system (Figs. 3–5) and our stage boundary estimates. However, this approach requires that the youngest $^{206}Pb/^{238}U$ date accurately represents the youngest zircon in the ash bed. Such an interpretation will be impacted by any minor Pb loss, and must consider the fact that even if there were a single age

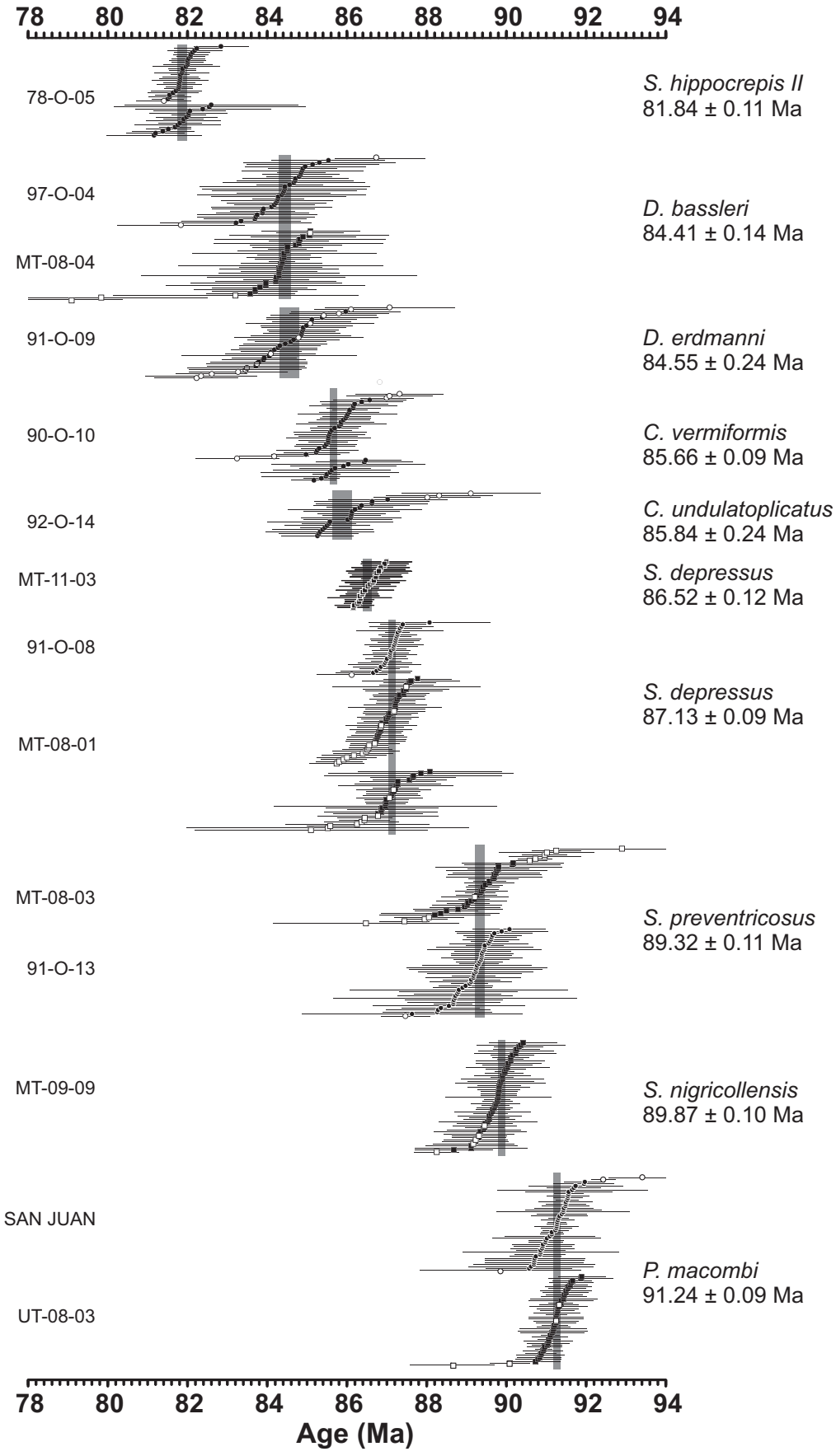

Figure 4. $^{40}Ar/^{39}Ar$ apparent ages determined from laser fusion analysis of sanidine crystals in volcanic ash beds spanning nine ammonite biozones (data from Table DR4.2 in the Data Repository [see footnote 1] and summarized in Table 1). Ages calculated relative to a Fish Canyon sanidine age of 28.201 Ma (Kuiper et al., 2008) with 2σ analytical uncertainties. Samples from the collection of Obradovich (1993) that were analyzed for this study are denoted by circles, whereas those from recently collected samples are marked by squares. Filled symbols are included in the calculation of a weighted mean age—shown by the vertical gray boxes—for each of the nine biozones. Open symbols have been excluded from the weighted mean age calculations. See Figure 2 for full taxonomic names.

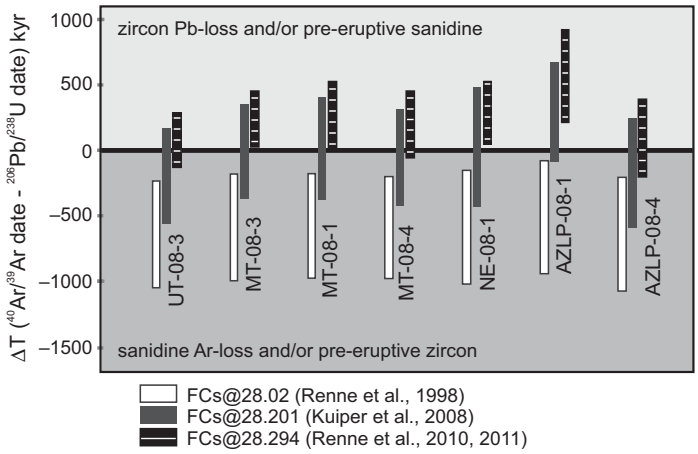

Figure 5. Summary of paired $^{206}Pb/^{238}U$ and $^{40}Ar/^{39}Ar$ results for seven Late Cretaceous ash beds, including four pairs from this study (Table 1) and three from Meyers et al. (2012; NE-08-1, AZLP-08-1, AZLP-08-4); error bars represent total uncertainties in both the $^{40}Ar/^{39}Ar$ and U-Pb dates combined in quadrature. Zircon U-Pb and sanidine $^{40}Ar/^{39}Ar$ ages that are equivalent will overlap with zero. Negative differences that plot below zero indicate either pre-eruptive zircon dates or argon loss from sanidine. Positive differences indicate either Pb loss from zircon or pre-eruptive sanidine dates. When the seven $^{40}Ar/^{39}Ar$ ages are calculated relative to 28.201 Ma Fish Canyon sanidine (FCs) (Kuiper et al., 2008), each overlaps zero. In contrast, among $^{40}Ar/^{39}Ar$ ages calculated relative to 28.294 Ma FCs (Renne et al., 2011), five plot with positive differences and two (AZLP-08-04 and UT-08-03) overlap zero. The five with positive values would require that, in the majority of these ash beds, zircons have experienced systematic Pb loss, or that sanidines record significant pre-eruptive residence periods in the source magma. These findings indicate that the FCs age (and decay constants) that results in the best agreement between the U-Pb and $^{40}Ar/^{39}Ar$ systems is that of Kuiper et al. (2008).

population in the ash bed, our sampling of this population will result in a normal distribution of $^{206}Pb/^{238}U$ dates around the true age; ad hoc selection of the youngest date could result in an age that is on the young side of the distribution. Thus, having considered the potential for minor Pb loss, inheritance, and recycling, we believe that the youngest coherent population best records temporal information pertinent to the time elapsed since eruption and deposition, and report preferred $^{206}Pb/^{238}U$ weighted mean ages of 91.37 ± 0.08/0.15 Ma (*P. macombi*), 89.37 ± 0.07/0.15 Ma (*S. preventricosus*), 87.11 ± 0.08/0.15 Ma (*S. depressus*), and 84.43 ± 0.09/0.15 Ma (*D. bassleri*) with MSWD values ranging between 1.3–2.3 (Fig. 3; Table 1). The listed uncertainties reflect the following sources: analytical / (analytical + tracer solution + decay constants); the latter value is the total uncertainty in each case.

$^{40}Ar/^{39}Ar$ Results

$^{40}Ar/^{39}Ar$ ages for ten bentonites representing eight ammonite biozones (three ashes, including *C. undulatoplicatus*, correspond to the *S. depressus* zone; Figs. 1, 2) were determined on the basis of 579 single- and multi-crystal laser-fusion experiments and two multi-crystal incremental heating experiments (Table 1; Fig. 4; complete data in Table DR4.2; Fig. DR4.3); the ages span late Turonian through early Campanian time. Following the logic of Schoene et al. (2013), we use the term "date" to denote the number calculated on the basis of the isotopic composition of a single measurement of argon from a crystal or group of crystals. Ages are then determined from the set of these dates, following the exclusion of analyses as follows: Outliers were removed from the age calculations owing to (1) "low" radiogenic $^{40}Ar^*$ (i.e., most cases <97% or 98% with the exception of samples MT-08-01, 90-O-10), (2) a K/Ca ratio significantly below the average of the population, and (3) apparent ages that were distinguishably older than the expected weighted mean age and 2σ uncertainty envelope. Given the analytical uncertainty associated with an individual apparent age, it may be challenging to resolve subtle inheritance or ^{40}Ar loss. However, automated systems can determine a large number of apparent dates per sample, as many as 75 in the case of MT-08-01, thereby enabling complex age distributions to be distinguished provided the variation exceeds the precision of the individual analyses, typically on the order of ~1%. Analyses excluded from the weighted mean age calculations may be clustered toward the low end of the apparent age distribution for a particular sample, for example in sample MT-09-09, or they may span the range of apparent dates, for example in samples 91-O-09 and MT-08-03 (Fig. 4). The weighted mean ages calculated for samples collected within each of the nine ammonite biozones fall in stratigraphic order between ca. 92 and 81 Ma (Fig. 4).

Fusion of single crystals was possible for ash beds that contained grains >150 µm in the *S. hippocrepis* II and *S. preventricosus* biozones (Table 1). Single sanidine crystals from twelve ash beds, processed from either Obradovich (1993) legacy samples or newly collected material, were too small (<150 µm) to yield signals 10 times larger than the blanks, thus fusion of 2–10 crystals per analysis was necessary (Table 1). The unimodal distribution of fusion dates in each sample motivates the use of weighted mean $^{40}Ar/^{39}Ar$ ages as the best estimate of time since eruption and deposition (Table 1; Fig. 4). Four biozones have paired $^{40}Ar/^{39}Ar$ ages from both a newly collected sample and an Obradovich (1993) legacy sample, and in each case the results are indistinguishable at the 2σ confidence level (Table 1). The dates determined from subsamples irradiated at different times are reported as separate lines in Table 1.

Table 1 gives the original age and uncertainty from Obradovich (1993), plus the new weighted mean ages and the uncertainties associated with the analysis only and the total uncertainty, both at ±2σ. To facilitate comparison, these ages are reported relative to the following calibrations of the FCs standard: (1) 28.02 Ma (Renne et al., 1998); (2) 28.201 Ma (Kuiper et al., 2008); and (3) 28.294 Ma (Renne et al., 2010, 2011).

Reconciling the U-Pb and $^{40}Ar/^{39}Ar$ Data Sets

The use of accurate radioisotopic data sets to determine how time is distributed in the strata of interest becomes ever more challenging as the level of temporal resolution increases. As noted above, our U-Pb zircon results highlight issues associated with pre-eruptive crystallization, whereas for $^{40}Ar/^{39}Ar$ results the lower precision of single crystal/aliquot measurements—coupled with the common assumption of a single population of normally distributed dates and uncertainties that justifies calculation of a weighted mean age for high-*n* data sets—may mask inheritance of older crystals and/or open-system behavior. Moreover, accuracy and precision of the $^{40}Ar/^{39}Ar$ method are tied to the

age and uncertainty of the neutron fluence standard and associated ^{40}K decay constants. In this section we review three pertinent calibrations of the $^{40}Ar/^{39}Ar$ system that have been proposed, but for which a consensus has yet to emerge. We then compare pairs of U-Pb and $^{40}Ar/^{39}Ar$ results from seven Cretaceous bentonites, including the four from this study and three presented in Meyers et al. (2012), to determine which of the three calibrations of the $^{40}Ar/^{39}Ar$ system are most appropriate for our use in estimating Cretaceous stage boundary ages. Such data sets are also pertinent to the long-term objective of minimizing bias between U-Pb and $^{40}Ar/^{39}Ar$ geochronometers.

The three proposed sets of ^{40}K total decay constant values and associated FCs neutron fluence standard ages include: (1) $5.543 \pm 0.020 \times 10^{-10}$ a^{-1} (Steiger and Jäger, 1977) for the FCs age of 28.02 ± 0.56 Ma (Renne et al., 1998), (2) $5.463 \pm 0.214 \times 10^{-10}$ a^{-1} (Min et al., 2000) for ages relative to the FCs age of 28.201 ± 0.046 Ma (Kuiper et al., 2008), and (3) $5.5305 \pm 0.0150 \times 10^{-10}$ a^{-1} for ages that are relative to a FCs age of 28.294 ± 0.072 Ma (Renne et al., 2010, 2011). The traditional 28.02 ± 0.56 Ma age of FCs is based on intercalibration against several standard minerals, including the primary (isotope dilution K-Ar) standard GA-1550 biotite (Renne et al., 1998). We report the ages here relative to the 28.02 Ma FCs age to illustrate that this calibration is no longer tenable for advancing the geological time scale (Schmitz, 2012).

Kuiper et al. (2008) used $^{40}Ar/^{39}Ar$-dated ash beds linked into an ATS that is tuned to match the Laskar et al. (2004) insolation solution, but that also requires correlating biostratigraphic events between distant stratigraphic sections in Spain and Morocco to arrive at an age for FCs of 28.201 ± 0.046 Ma. The Kuiper et al. (2008) experiment and results are supported by a more recent study using sanidines from ash beds of the astronomically tuned Faneromeni section in Crete (Rivera et al., 2011) and the revised calibration has been adopted for GTS2012 (Schmitz, 2012). Moreover, the youngest zircon $^{206}Pb/^{238}U$ date obtained from the Fish Canyon Tuff by Wotzlaw et al. (2013), using single-crystal CA-ID-TIMS methods and the EARTHTIME tracer solution, is 28.196 ± 0.038 Ma—identical to the astronomically calibrated age of FCs of Kuiper et al. (2008).

More recently, Renne et al. (2010, 2011) took a different approach—independent of astronomical dating—that optimized 16 pairs of $^{40}Ar/^{39}Ar$ and $^{206}Pb/^{238}U$ ages from rapidly cooled igneous rocks spanning from ca. 2.07 Ga to 17 Ma, together with ^{40}K activity data and K-Ar isotopic data, to revise the ^{40}K decay constants, which resulted in a FCs age of 28.294 ± 0.072 Ma.

Figure 5 shows seven Cretaceous $^{206}Pb/^{238}U$ ages and their paired $^{40}Ar/^{39}Ar$ ages (four from this study and three from Meyers et al. [2012]) calculated relative to the three pertinent FCs ages (using their respective ^{40}K decay constants). To estimate the total uncertainty of $^{40}Ar/^{39}Ar$ ages calculated relative to 28.02 Ma FCs, we note the very close agreement between an $^{40}Ar/^{39}Ar$ age of 40.4 ka for the Laschamp geomagnetic excursion that uses this standard age (Guillou et al., 2004) and the age of 40.7 ka (Singer et al., 2009) determined independently using the Kuiper et al. (2008) standard age, but also information from a U-Th isochron and the isotope stratigraphy of ice cores and marine sediments. The 300 yr difference between these two age determinations for the Laschamp excursion leads us to estimate the total uncertainty associated with the 28.02 Ma age for FCs at ~0.7%, not the much larger value highlighted by Kuiper et al. (2008). We find that if the $^{40}Ar/^{39}Ar$ ages are calculated relative to a 28.02 ± 0.20 Ma age for FCs (0.7% total uncertainty) they are younger than the $^{206}Pb/^{238}U$ zircon ages by ~600–800 k.y. If correct, this calibration implies that even the youngest zircons experienced very long magma residence times and/or that zircon inheritance is ubiquitous. Such long residence times are atypical for large silicic magmatic systems (e.g., Crowley et al., 2007; Simon et al., 2008; Wotzlaw et al., 2013) and more likely suggest a bias in the $^{40}Ar/^{39}Ar$ system as discussed by Kuiper et al. (2008) and Renne et al. (2010). Assuming that both the $^{206}Pb/^{238}U$ and $^{40}Ar/^{39}Ar$ ages in Figure 5 represent the time since eruption, all seven pairs support the 28.201 ± 0.046 Ma FCs age obtained by Kuiper et al. (2008). It might be argued that the $^{206}Pb/^{238}U$ ages of 91.37 ± 0.15 Ma from the *P. macombi* biozone (ash sample UT-08-03) and 94.37 ± 0.14 Ma from the *Watinoceras devonense* biozone (Meyers et al., 2012) are equally consistent with either the Kuiper et al. (2008) or Renne et al. (2011) calibration of the FCs standard. However, a choice of 28.294 Ma for FCs for four of the remaining six pairs clearly results in $^{40}Ar/^{39}Ar$ ages that are older than the $^{206}Pb/^{238}U$ ages, whereas a fifth sample only marginally matches the zircon age, thus suggesting: (1) sanidine closed to loss of Ar before zircon closed to loss of Pb, (2) Ar has a higher closure temperature in sanidine than does Pb in zircon, (3) most sanidine contains an inherited or excess ^{40}Ar component, and/or (4) all zircon is affected by Pb loss of broadly equal magnitude. We suggest that it is unlikely for Pb loss to produce coherent high-precision U-Pb populations such that results would show a plateau of dates in each of the bentonites, and that some of the dispersion within the U-Pb zircon data sets reflects age variation within single zircons, older dates reflecting a greater proportion of older cores (see Appendix DR3.1 for further discussion). Moreover, given our current knowledge of closure temperature and diffusion of argon in sanidine (e.g., Hora et al., 2010), we find it improbable that there is a ubiquitous and systematic inherited or excess $^{40}Ar^*$ component in the $^{40}Ar/^{39}Ar$ data sets obtained in this study. Thus, of the three different exercises that have attempted to calibrate the $^{40}Ar/^{39}Ar$ system using either astrochronology or U-Pb data as an independent variable, those of Kuiper et al. (2008) are most consistent with the U-Pb data obtained in this work and the study of Meyers et al. (2012), which include six pairs of U-Pb and $^{40}Ar/^{39}Ar$ ages spanning 94–84 Ma. Other recent U-Pb and $^{40}Ar/^{39}Ar$ data (Renne et al., 2013) have similarly been used to support the use of the Renne et al. (2010, 2011) $^{40}Ar/^{39}Ar$ calibration, however this data set is limited (one ash bed) and the relatively low single-date precision (0.4%–2%) makes it difficult to discern internal complexity, or lack thereof, within the zircon U-Pb data and thus its utility in distinguishing between the Kuiper et al. (2008) and Renne et al. (2010, 2011) calibrations. Thus, the remainder of our discussion is based on the Kuiper et al. (2008) FCs age of 28.201 ± 0.046 Ma calibration of the $^{40}Ar/^{39}Ar$ system.

Correlation Results

The stratigraphic position of dated ash layers, mainly sampled in Montana, is constrained by biostratigraphy (those ashes not sampled in the type sections reproduced in Fig. 2 are correlated to them based on associated index taxa). Although correlation of biozones from Montana to the Libsack core record, via the Pueblo outcrop section (Fig. 2), may add slight uncertainty due to lithostratigraphic variations, a larger uncertainty is associated with projecting the exact position of ashes into the 405 k.y. bandpass. These uncertainties are addressed as follows:

Scaphites preventricosus—Upper and lower boundaries of the biozone are very well constrained by index taxa in Montana and Pueblo (Appendix DR2) and the sampled ash is well constrained at the midpoint of the biozone in Montana (Fig. 2). Placing the correlation at the midpoint of the biozone in Pueblo locates it just above of the top of the Fort Hays Limestone. An ash bed occurring in the same position within the Libsack core is chosen as the optimal correlation point to the ATS. Although this is one of the best constrained ash correlations, an uncertainty of ±200 k.y. is applied to encompass adjacent ash beds in the Libsack core that could correlate to the ash bed sampled in Montana

(Table 2). In addition, hiatuses identified by missing inoceramid biozones occur within the lower part of the zone and at its upper boundary in the Pueblo section (and are inferred to occur in the Libsack core as well; Fig. 2).

Scaphites depressus—Upper and lower boundaries of the biozone are very well constrained by fossil data in Montana and Pueblo (Appendix DR2). The sampled ash, bed 110 in the section of Cobban et al. (1976), is also well constrained in the uppermost part of the *S. depressus* zone in Montana and it is correlated to the lower bed of a bentonite doublet in the basal part of the middle shale unit of Pueblo and Libsack (Fig. 2). An uncertainty of ±100 k.y., which ranges from the top of the underlying lower limestone to a position in the middle shale above the upper bentonite, is assigned to the correlation (Table 2).

Clioscaphites vermiformis—Boundaries of this biozone can be placed approximately in the Cobban et al. (1976) section (Fig. 2), but the location of the sampled ash within the zone is unconstrained due to the sample location (see Table DR1.1 and Figure DR1.2). Fossil data provide a better constraint in Pueblo, showing that the zone is limited to the upper part of the middle shale (Fig. 2), and projection of the zone to Libsack is based on limestone and bentonite correlations. This zone has the shortest duration of the five correlated biozones and an uncertainty value encompassing its entirety is ±70 k.y. (Table 2).

Desmoscaphites erdmanni—The upper and lower boundaries of this biozone are reasonably constrained by fossil data in Montana, but only the lower boundary is well constrained in Pueblo (Appendix DR2). As such, placement of the *D. erdmanni–D. bassleri* boundary in the Pueblo to Libsack part of the correlation is relatively uncertain. This boundary happens to coincide with the position of the *D. erdmanni* ash bed sampled in Montana. An uncertainty of ±200 k.y. would constrain it below the projected position of the *D. bassleri* ash, and is proposed as the best choice for this ash.

Desmoscaphites bassleri—The upper and lower boundaries of the biozone are reasonably well constrained by fossil data in Montana, but only the upper boundary is constrained in Pueblo where the LAD of *P. platinus* likely corresponds with the Santonian-Campanian boundary (Appendix DR2). The exact position of the sampled *D. bassleri* ash could not be determined in Montana so an uncertainty term that accommodates the entire zone (±200 k.y.) is applied.

DISCUSSION

The continued refinement of geological time scales, which requires integration of radioisotopic age data with well-defined stratigraphic units and their boundaries (i.e., biozones, stages, etc.), faces several discrete challenges. In addition to the contributions associated with radioisotopic measurements (including analytical, tracer or standard, and decay constant uncertainties) and the uncertainties due to interpolation techniques such as spline fitting (because radioisotopic data rarely coincide exactly with chronostratigraphic boundaries), there may be additional uncertainties stemming from the geological context of a time scale study (i.e., correlation commonly includes significant, but unquantified, assumptions). In order to determine the most accurate ages possible for the three stage boundaries considered in this research, we have determined new $^{40}Ar/^{39}Ar$ and $^{206}Pb/^{238}U$ ages that are more accurate and precise than past efforts, employed an astronomical age model for more accurate interpolation of ages, and explicitly quantified sources of uncertainty for each method and summed the values in a statistically valid manner. These results are presented in Table 3 and Figures 6 and 7.

Beyond the uncertainties associated with radioisotopic methods and geological correlation, discussed above, there are two additional sources of uncertainty that must be factored when using an ATS to interpolate stage boundary ages (or any other stratigraphic horizon in a study interval). The first concerns the accuracy of the 405 k.y. bandpass as a chronometer. Although the bandpass (Gaussian; 0.5–1.0 cycle m^{-1}) provides a superior interpolation tool because it maps time directly to stratigraphy and captures variations in sedimentation rate, multiple bandpass operations on a time series using a range of plausible parameters can yield a slightly variable distribution of peaks and troughs. In addition, climate and depositional system noise (Meyers et al., 2008; Meyers, 2012) can potentially distort the preserved eccentricity signal, and simulations that add random noise to a 405 k.y. record also show slight shifts in the position of peaks and troughs, generally not exceeding one-quarter of a long eccentricity cycle. To accommodate these potential uncertainties we include a value of ±100 k.y. for all age interpolations based on the 405 k.y. bandpass (Table 3).

The second source of uncertainty is the presence and relative magnitude of stratigraphic

TABLE 3. TURONIAN–CAMPANIAN STAGE BOUNDARY ESTIMATES USING $^{40}Ar/^{39}Ar$ AND U-PB DATA FROM FIVE ASH BEDS INTERPOLATED WITH THE 400 K.Y. BANDPASS ECCENTRICITY SIGNAL, INCORPORATING TOTAL RADIOISOTOPIC, GEOLOGIC, AND ORBITAL TIME SCALE UNCERTAINTIES

Radio-isotopic method	$^{40}Ar/^{39}Ar$* and $^{206}Pb/^{238}U$† ash bed ages		Stage boundary estimates					
			Turonian-Coniacian		Coniacian-Santonian		Santonian-Campanian	
	Age (Ma)	±2σ	Age (Ma)	±2σ§	Age (Ma)	±2σ§	Age (Ma)	±2σ§
Desmoscaphites bassleri								
$^{40}Ar/^{39}Ar$	84.41	±0.24	89.72	±0.46	86.39	±0.46	84.17	±0.46
$^{206}Pb/^{238}U$	84.43	±0.15	89.74	±0.38	86.41	±0.38	**84.19**	**±0.38**
Desmoscaphites erdmanni								
$^{40}Ar/^{39}Ar$	84.55	±0.37	89.66	±0.58	86.33	±0.58	84.11	±0.58
Clioscaphites vermiformis								
$^{40}Ar/^{39}Ar$	85.66	±0.19	89.55	±0.28	86.23	±0.28	84.01	±0.28
Scaphites depressus								
$^{40}Ar/^{39}Ar$	86.52	±0.33	89.82	±0.44	**86.49**	**±0.44**	84.27	±0.44
Scaphites preventricosus								
$^{40}Ar/^{39}Ar$	89.32	±0.24	89.70	±0.46	86.37	±0.46	84.15	±0.46
$^{206}Pb/^{238}U$	89.37	±0.15	**89.75**	**±0.38**	86.42	±0.38	84.20	±0.38

Note: All stage boundary estimates rely on the 405 k.y. bandpass cycle counts determined from the Libsack core. The preferred stage boundary age estimates based on the proximal ash method, shown in bold, employ the age determination with lowest uncertainty that is available for each boundary. Imported bentonite stratigraphy relies on the ammonite zonation of the Western Interior (Scott and Cobban, 1964; Cobban et al., 1976; Cobban, 1993; Leckie et al., 1997; Walaszczyk and Cobban, 2007). Preferred stage boundary ages in bold (see Fig. 7).

*$^{40}Ar/^{39}Ar$ weighted mean age of ash bed with full uncertainty (analytical, Fish Canyon sanidine [FCs] standard, and decay constant) reported relative to a FCs age of 28.201 Ma (Kuiper et al., 2008).

†U-Pb weighted mean age of ash bed with full uncertainty (analytical, ET535 tracer solution, decay constants of Jaffey et al. [1971]).

§Total uncertainty on stage boundary estimates include: full radioisotopic uncertainty (varies by sample), a 100 k.y. astronomical time scale uncertainty, and bentonite correlation uncertainty (varies by sample).

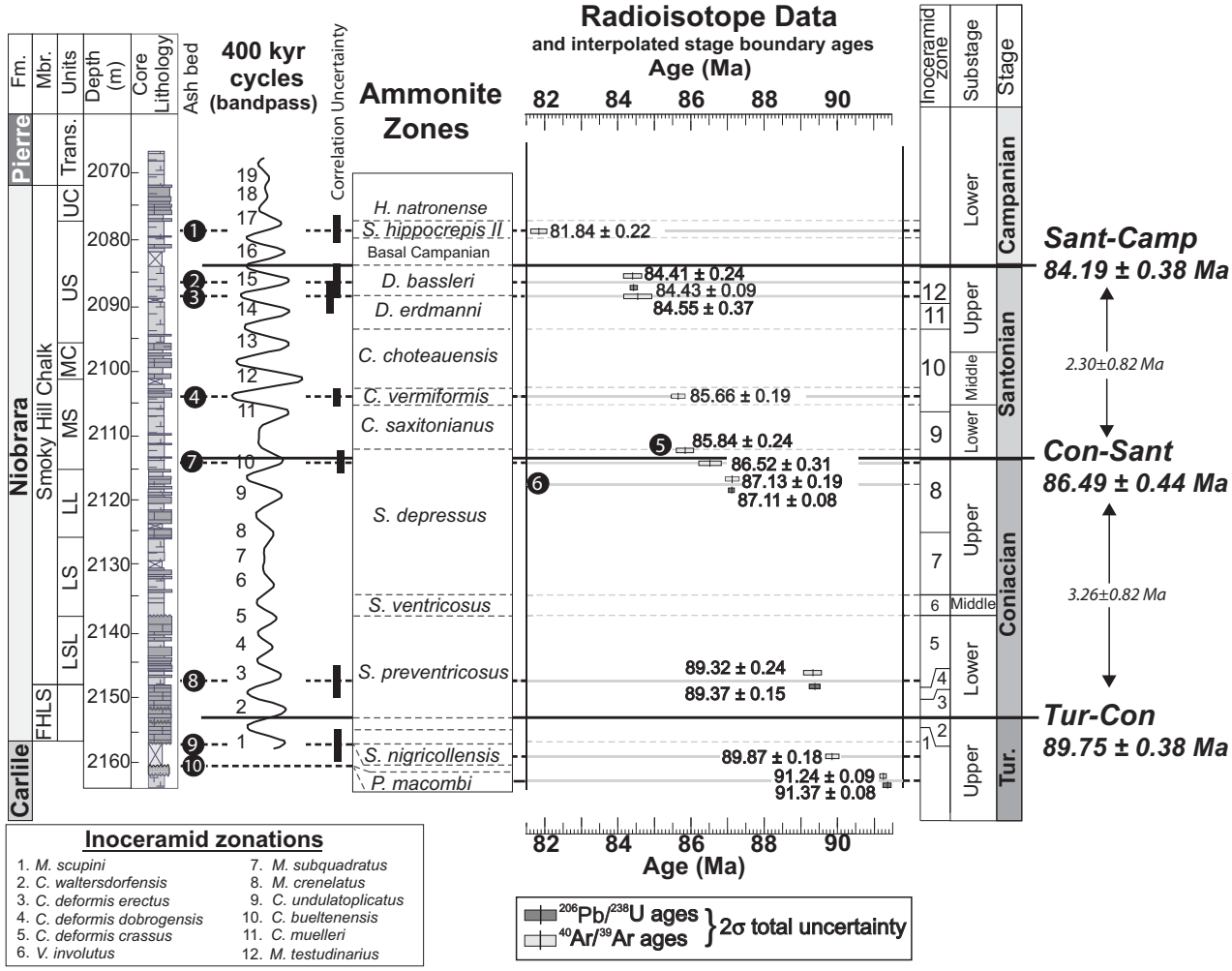

Figure 6. Lithostratigraphy, chronostratigraphy, and biostratigraphy of the Niobrara Formation (adapted from Locklair and Sageman, 2008). Formal and informal lithostratigraphy and biostratigraphic boundaries are from Walaszczyk and Cobban (2007), and projected bentonite locations are shown adjacent to the measured core section (black circles with numbers keyed to Fig. 1; the ash beds projected into Libsack astrochronology with reasonable confidence are listed next to the stratigraphic column). Stage boundary age estimates are interpolated from $^{40}Ar/^{39}Ar$ and U-Pb dated ash beds (gray rectangles) with elapsed time between ashes determined using the astronomical time scale (405 k.y. bandpass). See Figure 2 for abbreviations for Niobrara lithostratigraphic units. Tur—Turonian. See Figure 2 for full taxonomic names.

hiatuses, which may significantly impact the integration of radioisotopic and astrochronologic time scales. Astrochronologies in strata older than ca. 50 Ma are "floating" because they cannot be correlated to the Laskar et al. (2004, 2011) solutions. They can be "anchored," however, by reliable radioisotope dating and thereafter allow high-resolution age interpolation—*in the absence of significant hiatuses* (i.e., those with duration exceeding the age envelope due to other sources of uncertainty; in such cases, estimates of duration for a stratigraphic interval based on astrochronology will be significantly less than that determined by two radioisotope ages).

In general, spectral analysis of stratigraphic time series can allow tests of the hypothesis that orbital signals are expressed in the alternation of lithologic or other characteristics, and if so, provide the basis for developing a time scale that is independent of radioisotope data. But such analyses may not detect the presence of hiatuses. For example, if 4 m of a 20-m-thick interval preserves an excellent orbital record, but the remainder contains hiatuses, a corresponding simple power spectrum will indicate the presence of orbital frequencies and a bandpass of long eccentricity may show no evidence of hiatus. Evolutive techniques are more sensitive to the consistency of orbital signals through a section and can even provide a means to detect and quantify hiatuses, but if the duration of a gap is close to a whole integer multiple of the cycle being tracked, the hiatus may not be detected by spectral techniques (e.g., Meyers and Sageman, 2004).

Based on biostratigraphic data (described above and in Appendix DR2) there are several hiatuses within the Niobrara study interval that are not apparent in the 405 k.y. bandpass. Although a more detailed spectral analysis study focused on higher-frequency cycles might identify these stratigraphic gaps, this is beyond the scope of the present work (although the Niobrara hiatuses will be addressed presently). Our main objective is determination of the most accurate stage boundary ages that are possible given our new $^{40}Ar/^{39}Ar$, $^{206}Pb/^{238}U$, and astrochronologic information.

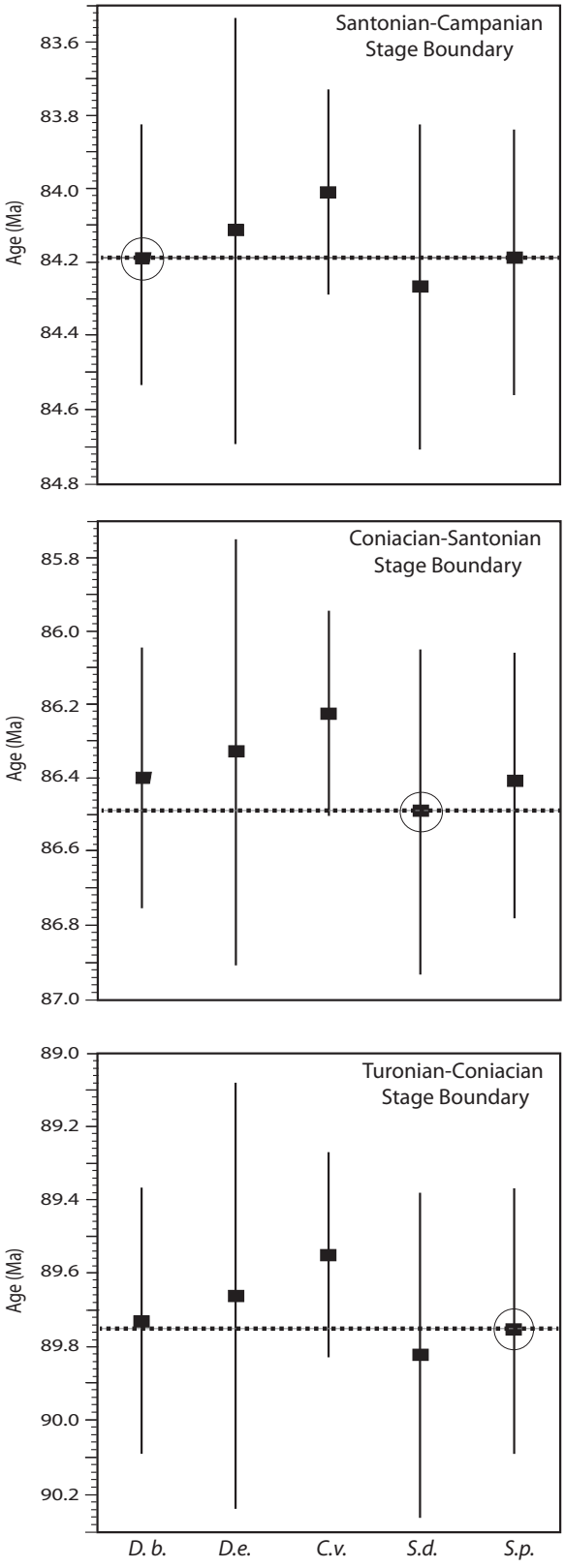

Figure 7. Interpolated age estimates for the three stage boundaries using each of five radioisotopically dated horizons, keyed to biozone (*D.b.—Desmoscaphites bassleri*; *D.e.—Desmoscaphites erdmanni*; *C.v.—Clioscaphites vermiformis*; *S.d.—Scaphites depressus*; *S.p.—Scaphites preventricosus*). The proximal ash value for each stage boundary is circled and this age is indicated by a thick dashed line. The total uncertainty for each interpolation is shown by vertical lines.

Stage Boundary Age Estimates and Stage Durations

The data used for determination of stage boundary ages are presented in Table 3. They include the $^{40}Ar/^{39}Ar$ and $^{206}Pb/^{238}U$ ages of ash horizons projected into the Libsack 405 k.y. bandpass, with their 2σ uncertainties, as well as the interpolated age of the stage boundaries using each projected ash horizon. In addition to the radioisotopic uncertainties, the interpolated stage boundary ages also include uncertainties associated with the 405 k.y. bandpass (±100 k.y.), and those due to correlation. With the exception of the correlation term, uncertainties are assumed to have a Gaussian distribution and are summed in quadrature; the correlation uncertainty is added to this sum to yield the total uncertainty of each stage boundary estimate. The most confident age determination for each stage boundary is based on interpolation from the dated ash horizon that is closest to the boundary; such estimates have the lowest degree of additive distortion. In addition, where both U-Pb and Ar/Ar data are available for the proximal ash, the age determination with lowest uncertainty is used as the basis for interpolation of the boundary age. These "proximal ash" ages are shown in bold in Table 3 and are the ages assigned to stage boundaries in Figure 6: 89.75 ± 0.38 Ma for the Turonian-Coniacian, 86.49 ± 0.44 Ma for the Coniacian-Santonian, and 84.19 ± 0.38 Ma for the Santonian-Campanian boundaries.

The three sources of temporal information presented in this study produce nearly identical results, given the uncertainties inherent in each method, on the order of 0.2–0.4 m.y. This provides remarkably strong support for the reliability of each method. In the case of the three paired $^{40}Ar/^{39}Ar$ and $^{206}Pb/^{238}U$ ages within the Niobrara interval, not only are the values identical within uncertainty, they differ by less than 50 k.y. (Tables 1 and 3) although we do acknowledge that using the data pairs to inform the choice of $^{40}Ar/^{39}Ar$ calibration introduces an element of co-variance. A floating astrochronology for the Libsack core was produced from the original resistivity data used by Locklair and Sageman (2008) and our result matches their 405 k.y. bandpass (typically with <100 k.y. offset of peaks/troughs). In Table 3 we present the results of stage boundary age interpolations using each of the dated ash horizons and the long eccentricity bandpass. The results are displayed graphically in Figure 7 (the favored proximal ash value is circled and represented by a thick dotted line; the total uncertainty for each interpolation is shown by a vertical line). These results indicate a very high level of agreement

in stage boundary age estimates using the bandpass to interpolate from different ash horizons.

Using our selected stage boundary ages (Table 3), the durations of the Coniacian and Santonian stages are 3.26 ± 0.35 and 2.30 ± 0.41 m.y., respectively. These estimates include uncertainty due to the astronomical time scale and correlation of ash beds, but as they are duration estimates we only apply the analytical uncertainty associated with radioisotopic ages. To directly compare astrochronologic and radioisotope estimates of duration for the combined stages consider the interval between the *S. preventricosus* and *D. bassleri* ash beds. The $^{206}Pb/^{238}U$ (4.94 ± 0.11 Ma), $^{40}Ar/^{39}Ar$ (4.91 ± 0.18 Ma), and ATS values (5.00 ± 0.38 Ma) overlap within uncertainty, providing additional confirmation of agreement between the three methods. These new results indicate a duration that is about a 10% longer, but well within the 20% uncertainty of the pioneering estimate of 4.43 ± 0.74 Ma by Obradovich (1993).

Niobrara Hiatuses

Hiatuses identified using biostratigraphic information occur in the Fort Hayes Limestone Member just above the Turonian-Coniacian boundary and at the top of the lower shale and limestone unit (Walaszczyk and Cobban, 2000, 2006, 2007). Also of note, there is a major late Turonian hiatus composed of multiple unconformities in the underlying Carlile Formation (Fisher et al., 1985; Merewether and Cobban, 1986). Comparison of the independent radioisotopic and astrochronologic data allows quantitative evaluation of these proposed discontinuities.

In an effort to constrain the duration of hiatus in the lower shale and limestone unit, we compare the new radioisotopic ages from *S. preventricosus* and *S. depressus* (which bracket the discontinuity) with the astronomically determined duration for the same interval; the two estimates are 2.84 ± 0.13 Ma (2σ radioisotopic analytical uncertainty) and 2.92 ± 0.44 Ma (2σ astronomical and correlation uncertainty), respectively. Although the average value for astronomical duration is greater than the average for radioisotopic duration, suggesting no hiatus, the maximum difference allowed by uncertainty is up to 0.5 m.y. To evaluate the duration of the hiatus in the Fort Hayes Limestone Member we compare the radioisotopic ages from *S. nigricollensis* (a biozone sampled in Montana that is stratigraphically younger than the multiple discontinuities of the Carlile Formation and which we project to the base of the Fort Hays ATS) and *S. preventricosus*. The radioisotopically determined duration is 0.51 ± 0.1 m.y. (2σ radioisotopic analytical uncertainty only, as the correlation uncertainty of *S. nigricollensis* is poorly constrained) and the ATS duration is 0.69 ± 0.34 m.y. (2σ astronomical and correlation uncertainty). Again, a larger value for the average astronomical duration suggests the hiatus is within the estimated uncertainty; the maximum allowed by uncertainty would be 0.26 m.y. In the event that the ATS duration for this interval was less than the radioisotopic duration and a larger hiatus was indicated, it would have been appropriate to add the missing time to the interpolated offset from the *S. preventricosus* age to obtain a more accurate value for the Turonian-Coniacian stage boundary.

Finally, the radioisotopic duration between ash beds of the late Turonian *P. macombi* and *S. nigricollensis* biozones of Montana is 1.37 ± 0.13 Ma (2σ analytical uncertainty, based on $^{40}Ar/^{39}Ar$ data), suggesting that a substantial amount of missing time is associated with this zone of multiple hiatuses in Colorado (as suggested by previous authors: Fisher et al., 1985; Merewether and Cobban, 1986). Filling in this temporal gap represents one of the most important targets for the completion of an astronomically tuned Cenomanian through early Campanian time scale that may unite the astrochronology of this study with that presented in Meyers et al. (2012).

CONCLUSIONS

A new radioisotopic framework for late Turonian through early Campanian time is based on $^{40}Ar/^{39}Ar$ and $^{206}Pb/^{238}U$ data from nine volcanic ash beds that occur within the Cretaceous ammonite biostratigraphy of Cobban (1993). Pairing $^{206}Pb/^{238}U$ and $^{40}Ar/^{39}Ar$ data sets from seven ash beds, including three from the Cenomanian and Turonian (Meyers et al., 2012), supports the astronomical age of 28.201 ± 0.046 Ma for the Fish Canyon sanidine standard (Kuiper et al., 2008). Five ages from radioisotopically dated ash beds in Montana were projected at the sub-biozonal scale into the astrochronology of the Libsack 43-27 core, Denver Basin, allowing improved interpolation of stage boundary ages. The most proximal ash to each stage boundary (two of which included both $^{40}Ar/^{39}Ar$ and $^{206}Pb/^{238}U$ ages) was used to estimate stage boundary ages with highest confidence; they are 89.75 ± 0.38 Ma for the Turonian-Coniacian, 86.49 ± 0.44 Ma for the Coniacian-Santonian, and 84.19 ± 0.38 Ma for the Santonian-Campanian boundaries. The latter estimate for the Santonian-Campanian stage boundary also precisely marks the termination of the Cretaceous long normal chron 34n and is 580 k.y. older than the age recently proposed by Ogg and Hinnov (2012), which is based, in part, on an early presentation of the data we have reported here.

Our results: (1) improve the precision of stage boundary ages by an order of magnitude (total uncertainty) compared to earlier estimates (e.g., GTS04 by Ogg et al., 2004; the GTS12 ages in Ogg and Hinnov [2012] were based on an early version of this manuscript), (2) provide both $^{40}Ar/^{39}Ar$ and $^{206}Pb/^{238}U$ radioisotopic tiepoints that are biostratigraphically constrained, thereby helping to anchor astrochronologic age models currently under investigation, (3) revise the age of the termination of the Cretaceous normal super chron to ca. 84.2 Ma, and (4) present new approaches for the determination and calculation of astrochronologic and geologic uncertainties in the development of integrated time scales.

ACKNOWLEDGMENTS

This paper comprises, in part, the Master of Science thesis research of Sarah Siewert at University of Wisconsin–Madison. We would like to thank Nicola Atkinson for assistance with U-Pb analyses and Dylan Loss, Dylan Colon, Alexandra Macho, and Kim Hoxie for their help during sample preparation. Kevin McKinney, Bill Cobban, and Al Merewether of the USGS in Denver were instrumental in helping to locate ash bed outcrops for sampling and provided guidance about the position of ash beds within ammonite zones. The research was financially supported by a BP Research Assistantship and Shell undergraduate research award to Siewert, a University of Wisconsin–Madison Graduate School Vilas Associate award to Singer, and NSF grant EAR-0959108 (Singer, Meyers, and Sageman) and NIGFSC award IP/1011/1107 (Condon). Dr. E. "Gus" Gustason is thanked for facilitating the gift of the Libsack core from Encana Inc. to Northwestern University.

REFERENCES CITED

Agterberg, F.P., 1994, Estimation of the Mesozoic geological time scale: Mathematical Geology, v. 26, p. 857–876, doi:10.1007/BF02083122.

Arthur, M.A., and Dean, W.E., 1991, An holistic geochemical approach to cyclomania: Examples from Cretaceous pelagic limestone sequences, *in* Einsele, G., Ricken, W., and Seilacher, A., eds., Cycles and Events in Stratigraphy: Berlin, Springer-Verlag, p. 126–166.

Cobban, W.A., 1964, The Late Cretaceous cephalopod *Haresiceras* Reeside and its possible origin: U.S. Geological Survey Professional Paper 454-I, 21 p., 3 pl.

Cobban, W.A., 1969, The Late Cretaceous ammonites Scaphites leei Reeside and Scaphites hippocrepis (DeKay) in the western interior of the United States: U.S. Geological Survey Professional Paper 619, 29 p.

Cobban, W.A., 1993, Diversity and distribution of Late Cretaceous ammonites, Western Interior, U.S., *in* Caldwell, W.G.E., and Kauffman, E.G., eds., Evolution of the Western Interior Basin: Geological Association of Canada Special Paper 39, p. 435–452.

Cobban, W.A., Erdmann, C.E., Lemke, R.W., and Maughan, E.K., 1976, Type sections and stratigraphy of the members of the Blackleaf and Marias River Formations (Cretaceous) of the Sweetgrass Arch, Montana: U.S. Geological Survey Professional Paper 974, 66 p.

Cobban, W.A., Dyman, T.S., and Porter, K.W., 2005, Paleontology and stratigraphy of upper Coniacian–middle Santonian ammonite zones and application to erosion surfaces and marine transgressive strata in Montana and Alberta: Cretaceous Research, v. 26, p. 429–449, doi:10.1016/j.cretres.2005.01.007.

Cobban, W.A., Walaszczyk, I., Obradovich, J.D., and McKinney, K.C., 2006, A USGS zonal table for the Upper Cretaceous middle Cenomanian–Maastrichtian of the Western Interior of the United States based on ammonites, inoceramids, and radiometric ages: U.S. Geological Survey Open-File Report 2006-1250, 46 p.

Condon, D., Schoene, B., Bowring, S.A., Parrish, R., McLean, N., Noble, S., and Crowley, Q., 2007, EARTHTIME: Isotopic tracers and optimized solutions for high-precision U-Pb ID-TIMS geochronology [abs.]: Eos (Transactions, American Geophysical Union), v. 88, no. 52, V41E-06.

Crowley, J.L., Schoene, B., and Bowring, S.A., 2007, U-Pb dating of zircon in the Bishop Tuff at the millennial scale: Geology, v. 35, p. 1123–1126, doi:10.1130/G24017A.1.

Dean, W.E., and Arthur, M.A., 1998, Geochemical expression of cyclicity in Cretaceous pelagic limestone sequences: Niobrara Formation, Western Interior Seaway, *in* Dean, W.E., and Arthur, M.A., eds., Stratigraphy and Paleoenvironments of the Cretaceous Western Interior Seaway, U.S.A.: SEPM (Society for Sedimentary Geology) Concepts in Sedimentology and Paleontology 6, p. 227–255.

Duffield, W.A., and Dalrymple, G.B., 1990, The Taylor Creek Rhyolite of New Mexico: A rapidly emplaced field of lava domes and flows: Bulletin of Volcanology, v. 52, p. 475–487, doi:10.1007/BF00268927.

Erdmann, C.E., Gist, J.T., Nordquist, J.W., and Beer, G.W., 1947, Map of the areal and structural geology of T. 35 N., R. 3 W., Toole County, Montana, showing oil pools in West Kevin district, Kevin-Sunburst oil field: U.S. Geological Survey unnumbered map.

Fischer, A.G., 1980, Gilbert—Bedding rhythms and geochronology, *in* Yochelson, E.I., ed., The Scientific Ideas of G.K. Gilbert: Geological Society of America Special Paper 183, p. 93–104, doi:10.1130/SPE183-p93.

Fischer, A.G., 1993, Cyclostratigraphy of Cretaceous chalk-marl sequences, *in* Caldwell, W.G.E, and Kauffman, E.G., eds., Evolution of the Western Interior Basin: Geological Association of Canada Special Paper 39, p. 283–295.

Fischer, A.G., and Bottjer, D.J., 1991, Orbital forcing and sedimentary sequences: Journal of Sedimentary Petrology, v. 61, p. 1063–1069.

Fischer, A.G., Herbert, T., and Premoli-Silva, L., 1985, Carbonate bedding cycles in Cretaceous pelagic and hemipelagic sediments, *in* Pratt, L.M., Kauffman, E.G., and Zelt, F.B., eds., Fine-Grained Deposits and Biofacies of the Cretaceous Western Interior Seaway: Evidence of Cyclic Sedimentary Processes: SEPM (Society for Sedimentary Geology) Field Trip Guidebook 4, p. 1–10.

Fisher, C.G., Kauffman, E.G, and Wilhelm, L.V.H., 1985, The Niobrara transgressive hemicyclothem in central and eastern Colorado: The anatomy of a multiple disconformity, *in* Pratt, L.M., Kauffman, E.G., and Zelt, F.B., eds., Fine-Grained Deposits and Biofacies of the Cretaceous Western Interior Seaway: Evidence of Cyclic Sedimentary Processes: SEPM (Society for Sedimentary Geology) Field Trip Guidebook 4, p. 184–198.

Gilbert, G.K., 1895, Sedimentary measurement of geologic time: Geology, v. 3, p. 121–127, doi:10.1086/607150.

Gradstein, F.M, Ogg, J.G., Schmitz, M.D., and Ogg, G., 2012, The Geologic Time Scale 2012: Boston, USA, Elsevier, doi:10.1016/B978-0-444-59425-9.00004-4.

Grifi, M.D., Plint, A.G., and Walaszczyk, I., 2013, Rapidly changing styles of subsidence revealed by high-resolution mudstone allostratigraphy: Coniacian of Sweetgrass Arch area, southern Alberta and northern Montana: Canadian Journal of Earth Sciences, v. 50, p. 439–461, doi:10.1139/cjes-2012-0031.

Grippo, A., Fischer, A.G., Hinnov, L.A., Herbert, T.D., and Premoli-Silva, I., 2004, Cyclostratigraphy and chronology of the Albian stage (Piobbico core, Italy), *in* d'Argenio, B., Fischer, A.G., Premoli-Silva, I., Weissert, H., and Ferreri, V., eds., Cyclostratigraphy: Approaches and Case Histories: Society for Sedimentary Geology Special Publication 81, p. 57–81.

Guillou, H., Singer, B.S., Laj, C., Kissell, C., Scaillet, S., and Jicha, B.R., 2004, On the age of the Laschamp Event: Earth and Planetary Science Letters, v. 227, p. 331–343, doi:10.1016/j.epsl.2004.09.018.

Hattin, D.E., 1982, Stratigraphy and depositional environment of Smoky Hill Chalk Member, Niobrara Chalk (Upper Cretaceous) of the type area, western Kansas: Kansas State Geological Survey Bulletin 225, 108 p.

Hinnov, L.A., and Ogg, J.G., 2007, Cyclostratigraphy and the Astronomical Time Scale: Stratigraphy, v. 4, no. 2–3, p. 239–251.

Hinnov, L.A., and Hilgen, F.J., 2012, Cyclostratigraphy and astrochronology, *in* Gradstein, F.M., Ogg, J.G., Schmitz, M., and Ogg, G., eds., The Geologic Time Scale 2012: Berlin, Elsevier, p. 63–83.

Hora, J.M., Singer, B.S., Jicha, B.J., Beard, B.L., Johnson, C.M., De Silva, S., and Salisbury, M., 2010, Volcanic biotite-sanidine $^{40}Ar/^{39}Ar$ age discordances reflect Ar partitioning and pre-eruption closure in biotite: Geology, v. 38, p. 923–926, doi:10.1130/G31064.1.

Huang, C., Hinnov, L., Fischer, A.G., Grippo, A., and Herbert, T., 2010, Astronomical tuning of the Aptian Stage from Italian reference sections: Geology, v. 38, p. 899–902, doi:10.1130/G31177.1.

Jaffey, A.H., Flynn, K.F., Glendenin, L.E., Bentley, W.C., and Essling, A.M., 1971, Precision measurement of half-lives and specific activities of ^{235}U and ^{238}U: Physical Review, v. C4, p. 1889–1906.

Kowallis, B.J., Christiansen, E.H., Deino, A.L., Kunk, M.J., and Heaman, L.M., 1989, Age of the Cenomanian-Turonian boundary in the Western Interior of the United States: Cretaceous Research, v. 16, 109–129.

Kuiper, K.F., Deino, A., Hilgen, F.J., Krijgsman, W., Renne, P.R., and Wijbrans, J.R., 2008, Synchronizing rock clocks of Earth history: Science, v. 320, p. 500–504, doi:10.1126/science.1154339.

Landman, N.H., and Cobban, W.A., 2007, Redescription of the Late Cretaceous (late Santonian) ammonite *Desmoscaphites bassleri* Reeside, 1927, from the Western Interior of North America: Rocky Mountain Geology, v. 42, p. 67–94, doi:10.2113/gsrocky.42.2.67.

Laskar, J., Robutel, P., Joutel, F., Gastineau, M., Correia, A.C.M., and Levrard, B., 2004, A long-term numerical solution for the insolation quantities of the Earth: Astronomy & Astrophysics, v. 428, p. 261–285, doi:10.1051/0004-6361:20041335.

Laskar, J., Fienga, A., Gastineau, M., and Manche, H., 2011, La2010: A new orbital solution for the long-term motion of the Earth: Astronomy and Astrophysics, v. 532, A89, 15 p.

Leckie, R.M., Kirkland, J.I., and Elder, W.P., 1997, Stratigraphic framework and correlation of a principal reference section of the Mancos Shale (Upper Cretaceous), Mesa Verde, Colorado, *in* Anderson, O.J., Kues, B.S., and Lucas, S.G., eds., Mesozoic Geology and Paleontology of the Four Corners Region: New Mexico Geological Society 48th Field Conference Guidebook, p. 163–216.

Locklair, R.E., 2007, Causes and consequences of marine carbon burial: Examples from the Cretaceous Niobrara Formation and the Permian Brushy Canyon Formation [unpublished Ph.D. thesis]: Evanston, Illinois, Northwestern University, 515 p.

Locklair, R.E., and Sageman, B.B., 2008, Cyclostratigraphy of the Upper Cretaceous Niobrara Formation, Western Interior, U.S.A.: A Coniacian-Santonian orbital timescale: Earth and Planetary Science Letters, v. 269, p. 540–553, doi:10.1016/j.epsl.2008.03.021.

Logan, W.N., 1897, The Upper Cretaceous of Kansas: Kansas University Geological Survey, v. 2, p. 195–234.

Longman, M.W., Luneau, B.A., and Landon, S.M., 1998, Nature and distribution of Niobrara lithologies in the Cretaceous Western Interior Seaway of the Rocky Mountain region: The Mountain Geologist, v. 35, p. 137–170.

Ludwig, K.R., 2003, User's manual for Isoplot 3.00: A geochronological toolkit for Microsoft Excel: Berkeley Geochronology Center Special Publication 4, 70 p.

Mattinson, J.M., 2005, Zircon U/Pb chemical abrasion (CA-TIMS) method: Chemical Geology, v. 220, p. 47–66, doi:10.1016/j.chemgeo.2005.03.011.

Mattinson, J.M., 2010, Analysis of the relative decay constants of ^{235}U and ^{238}U by multi-step CA-TIMS measurements of closed-system natural zircon samples: Chemical Geology, v. 275, p. 186–198, doi:10.1016/j.chemgeo.2010.05.007.

Meek, F.B., and Hayden, F.V., 1861, Descriptions of new Silurian (Primordial), Jurassic, Cretaceous, and Tertiary fossils collected in Nebraska by the exploring expedition under the command of Capt. William F. Raynolds, U.S. Topographical Engineers, with some remarks on the rocks from which they were obtained: Proceedings, Academy of Natural Sciences of Philadelphia, v. 13, p. 415–447.

Merewether, E.A., and Cobban, W.A., 1986, Biostratigraphic units and tectonism in the mid-Cretaceous foreland of Wyoming, Colorado, and adjoining areas, *in* Peterson, J.A., ed., Paleotectonics and Sedimentation: American Association of Petroleum Geologists Memoir 41, p. 443–468.

Meyers, S.R., 2012, Seeing Red in Cyclic Stratigraphy: Spectral Noise Estimation for Astrochronology: Paleoceanography, 27, PA3228, doi:10.1029/2012PA002307.

Meyers, S.R., and Sageman, B.B., 2004, Detection, quantification, and significance of hiatuses in pelagic and hemipelagic strata: Earth and Planetary Science Letters, v. 224, p. 55–72, doi:10.1016/j.epsl.2004.05.003.

Meyers, S.R., Sageman, B., and Hinnov, L., 2001, Integrated quantitative stratigraphy of the Cenomanian-Turonian Bridge Creek Limestone Member using evolutive harmonic analysis and stratigraphic modeling: Journal of Sedimentary Research, v. 71, p. 628–644, doi:10.1306/012401710628.

Meyers, S.R, Sageman, B.B., and Pagani, M., 2008, Resolving Milankovitch: Consideration of signal and noise: American Journal of Science, v. 308, p. 770–786.

Meyers, S.R., Siewert, S.E., Singer, B.S., Sageman, B.B., Condon, D., Obradovich, J.D., Jicha, B.R., and Sawyer, D.A., 2012, Intercalibration of radioisotopic and astrochonologic time scales for the Cenomanian-Turonian boundary interval, Western Interior Basin, USA: Geology, v. 40, p. 7–10, doi:10.1130/G32261.1.

Miller, J.S., Matzel, J.E.P., Miller, C.F., Burgess, S.D., and Miller, R.B., 2007, Zircon growth and recycling during the assembly of large, composite arc plutons: Journal of Volcanology and Geothermal Research, v. 167, p. 282–299, doi:10.1016/j.jvolgeores.2007.04.019.

Min, K., Mundil, R., Renne, P.R., and Ludwig, K.R., 2000, A test for systematic errors in $^{40}Ar/^{39}Ar$ geochronology through comparison with U/Pb analysis of a 1.1-Ga rhyolite: Geochimica et Cosmochimica Acta, v. 64, p. 73–98, doi:10.1016/S0016-7037(99)00204-5.

Obradovich, J., 1993, A Cretaceous time scale, *in* Caldwell, W.G.E., and Kauffman, E.G., eds., Evolution of the Western Interior Basin: Geological Society of Canada Special Paper 39, p. 379–396.

Ogg, J.G., and Hinnov, L.A., 2012, Chapter 27, Cretaceous, *in* Gradstein, F., Ogg, J., Schmitz, M., and Ogg, G., eds., The Geologic Time Scale 2012: Oxford, Elsevier, 793–853.

Ogg, J.G., Agterberg, F.P., and Gradstein, F.M., 2004. The Cretaceous Period, *in* Gradstein, F.M., Ogg, J.G., and Smith, A.G., eds., A Geologic Time Scale 2004: New York, Cambridge University Press, p. 344–383.

Pratt, L.M., Arthur, M.A., Dean, W.E., and Scholle, P.A., 1993, Paleoceanographic cycles and events during the Late Cretaceous in the Western Interior Seaway of North America, *in* Caldwell, W.G.E., and Kauffman, E.G., eds., Evolution of the Western Interior Basin: Geological Association of Canada Special Paper 39, p. 333–354.

Renne, P.R., Swisher, C.C., Deino, A.L., Karner, D.B., Owens, T.L., and DePaolo, D.J., 1998, Intercalibration of standards, absolute ages and uncertainties in $^{40}Ar/^{39}Ar$ dating: Chemical Geology, v. 145, p. 117–152, doi:10.1016/S0009-2541(97)00159-9.

Renne, P.R., Mundil, R., Balco, G., Min, K., and Ludwig, K.R., 2010, Joint determination of ^{40}K decay constants and $^{40}Ar^*/^{40}K$ for the Fish Canyon sanidine standard, and improved accuracy for $^{40}Ar/^{39}Ar$ geochronology: Geochimica et Cosmochimica Acta, v. 74, p. 5349–5367, doi:10.1016/j.gca.2010.06.017.

Renne, P.R., Balco, G., Mundil, R., and Min, K., 2011, Response to the comment by W.H. Schwarz et al. on "Joint determination of ^{40}K decay constants and $^{40}Ar^*/^{40}K$ for the Fish Canyon sanidine standard, and improved accuracy for $^{40}Ar/^{39}Ar$ geochronology" by P.R. Renne et al. (2010): Geochimica et Cosmochimica Acta, v. 75, p. 5097–5100, doi:10.1016/j.gca.2011.06.021.

Renne, P.R., Deino, A.L., Hilgen, F.J., Kuiper, K.F., Mark, D.F., Mitchell, W.S., III, Morgan, L.E., Mundil, R., and Smit, J., 2013, Time scales of critical events around the Cretaceous-Paleogene boundary: Science, v. 339, p. 684–687, doi:10.1126/science.1230492.

Ricken, W., 1994, Complex rhythmic sedimentation related to third-order sea-level variations: Upper Cretaceous, Western Interior Basin, USA, *in* de Boer, P.L., and Smith, D.G., eds., Orbital Forcing and Cyclic Sequences: International Association of Sedimentologists Special Publication 19, p. 167–193.

Rivera, T.A., Storey, M., Zeeden, C., Hilgen, F.J., and Kuiper, K., 2011, A refined astronomically calibrated $^{40}Ar/^{39}Ar$ age for Fish Canyon sanidine: Earth and Planetary Science Letters, v. 311, p. 420–426, doi:10.1016/j.epsl.2011.09.017.

Roberts, L.N.R., and Kirschbaum, M.A., 1995, Paleogeography of the Late Cretaceous of the Western Interior of middle North America—Coal distribution and sediment accumulation: U.S. Geological Survey Professional Paper 1561, 115 p.

Sageman, B.B., Rich, J., Arthur, M.A., Birchfield, G.E., and Dean, W.E., 1997, Evidence for Milankovitch periodicities in Cenomanian-Turonian lithologic and geochemical cycles, Western Interior U.S.A.: Journal of Sedimentary Research, v. 67, p. 286–301.

Sageman, B.B., Meyers, S.R., and Arthur, M.A., 2006, Orbital time scale and new C-isotope record for Cenomanian-Turonian boundary stratotype: Geology, v. 34, p. 125–128, doi:10.1130/G22074.1.

Savrda, C.E., and Bottjer, D.J., 1989, Trace fossil model for reconstructing oxygenation histories of ancient marine bottom waters: Application to Upper Cretaceous Niobrara Formation, Colorado: Palaeogeography, Palaeoclimatology, Palaeoecology, v. 74, p. 49–74, doi:10.1016/0031-0182(89)90019-9.

Schaltegger, U., Brack, P., Ovtcharova, M., Peytcheva, I., Schoene, B., Stracke, A., Marocchi, M., and Bargossi, G.M., 2009, Zircon and titanite recording 1.5 million years of magma accretion, crystallization and initial cooling in a composite pluton (southern Adamello batholiths, northern Italy): Earth and Planetary Science Letters, v. 286, p. 208–218, doi:10.1016/j.epsl.2009.06.028.

Schmitz, M.D., 2012, Radiogenic isotope geochronology, *in* Gradstein, F.M., Ogg, J.G., Schmitz, M.D., and Ogg, G.M., eds., The Geologic Time Scale 2012: Oxford, Elsevier , v. 1, p. 115–126.

Schoene, B., Guex, J., Bartolini, A., Schaltegger, U., and Blackburn, T., 2010, Correlating the end-Triassic mass extinction and flood basalt volcanism at the 100 ka level: Geology, v. 38, p. 387–390, doi:10.1130/G30683.1.

Schoene, B., Condon, D.J., Morgan, L., and McLean, N., 2013, Precision and accuracy in geochronology: Elements, v. 9, p. 19–24, doi:10.2113/gselements.9.1.19.

Scott, G.R., and Cobban, W.A., 1964, Stratigraphy of the Niobrara Formation at Pueblo, Colorado: U.S. Geological Survey Professional Paper 454-L, 27 p.

Seiwert, S.E., 2011, Integrating $^{40}Ar/^{39}Ar$, U-Pb, and astronomical clocks in the Cretaceous Niobrara Formation, [M.S. thesis]: University of Wisconsin–Madison, 70 p., ocn744451007.

Simon, J.I., Renne, P.R., and Mundil, R., 2008, Implications of pre-eruptive magmatic histories of zircons for U-Pb geochronology of silicic extrusions: Earth and Planetary Science Letters, v. 266, p. 182–194, doi:10.1016/j.epsl.2007.11.014.

Singer, B.S., Guillou, H., Jicha, B.R., Laj, C., Kissel, C., Beard, B.L., and Johnson, C.M., 2009, $^{40}Ar/^{39}Ar$, K-Ar and ^{230}Th-^{238}U dating of the Laschamp excursion: A radioisotopic tie-point for ice core and climate chronologies: Earth and Planetary Science Letters, v. 286, p. 80–88, doi:10.1016/j.epsl.2009.06.030.

Skelton, P.W., ed., 2003, The Cretaceous World: Cambridge, Cambridge University Press, 360 p.

Smith, M.E., Carroll, A.R., and Singer, B.S., 2008, Synoptic reconstruction of a major ancient lake system: Eocene Green River Formation, western United States: Geological Society of America Bulletin, v. 120, p. 54–84, doi:10.1130/B26073.1.

Smith, M.E., Chamberlain, K.R., Singer, B.S., and Carroll, A.R., 2010, Eocene clocks agree: Coeval $^{40}Ar/^{39}Ar$, U-Pb, and astronomical ages from the Green River Formation: Geology, v. 38, p. 527–530, doi:10.1130/G30630.1.

Steiger, R.H., and Jäger, E., 1977, Subcommission on geochronology: Convention on the use of decay constants in geo- and cosmochronology: Earth and Planetary Science Letters, v. 36, p. 359–362, doi:10.1016/0012-821X(77)90060-7.

Thomson, D.J., 1982, Spectrum estimation and harmonic analysis: IEEE Proceedings, v. 70, p. 1055–1096, doi:10.1109/PROC.1982.12433.

Walaszczyk, I., and Cobban, W.A., 1999, The Turonian-Coniacian boundary in the United States Western Interior: Acta Geologica Polonica, v. 48, p. 495–507.

Walaszczyk, I., and Cobban, W.A., 2000, Inoceramid faunas and biostratigraphy of the upper Turonian–lower Coniacian of the Western Interior of the United States: Palaeontological Association [London] Special Paper 64, 118 p.

Walaszczyk, I., and Cobban, W.A., 2006, Palaeontology and stratigraphy of the Middle-Upper Coniacian and Santonian inoceramids of the US Western Interior: Acta Geologica Polonica, v. 56, p. 241–348.

Walaszczyk, I., and Cobban, W.A., 2007, Inoceramid fauna and biostratigraphy of the upper Middle Coniacian–lower Middle Santonian of the Pueblo Section (SE Colorado, US Western Interior): Cretaceous Research, v. 28, p. 132–142, doi:10.1016/j.cretres.2006.05.024.

Wendt, I., and Carl, C., 1991, The statistical distribution of the mean squared weighted deviation: Chemical Geology, v. 86, p. 275–285.

Wotzlaw, J.-F., Schaltegger, U., Frick, D.A., Dungan, M.A., Gerdes, A., and Gunther, D., 2013, Tracking the evolution of large-volume silicic magma reservoirs from assembly to super-eruption: Geology, v. 41, p. 867–870, doi:10.1130/G34366.1.

Science Editor: Christian Koeberl
Associate Editor: Cinzia Cervato

Manuscript Received 25 May 2013
Revised Manuscript Received 23 November 2013
Manuscript Accepted 22 January 2014

Printed in the USA